



OPEN

## Eco-friendly synthesis of bioactive silver nanoparticles from black roasted gram (*Cicer arietinum*) for biomedical applications

Muhammad Awais Farooqi<sup>1,6</sup>, Sungmin Bae<sup>2,6</sup>, Sehui Kim<sup>3</sup>, Sungeun Bae<sup>2</sup>, Farzana Kausar<sup>4</sup>, Hafiz Muhammad Umer Farooqi<sup>5</sup>, Chang Gu Hyun<sup>2</sup> & Chul Ung Kang<sup>1</sup>

Green synthesis leverages biological resources such as plant extracts to produce cost-effectively and environmentally friendly NPs. In our study, silver nanoparticles (AgNPs) are biosynthesized using blank roasted grams (*Cicer arietinum*) as reducing agents. CA-AgNPs were characterized by a characteristic surface plasmon resonance (SPR) peak at 224 nm in the UV-Vis spectrum. FTIR analysis revealed functional groups with O-H stretching at 3410 cm<sup>-1</sup>, C-H stretching at 2922 cm<sup>-1</sup>, and C=O stretching at 1635 cm<sup>-1</sup>. XRD patterns exhibited sharp peaks at 33.2°, 38.4°, 55.7°, and 66.6°, confirming high crystallinity. Morphological analysis through FESEM indicated spherical CA-AgNPs averaging 500 nm in size, with EDS revealing Ag at 97.51% by weight. Antimicrobial assays showed zones of inhibition of 14 mm against *Candida albicans*, 18 mm against *Escherichia coli*, and 12 mm against *Propionibacterium acnes*. The total phenolic content of CA-AgNPs was 26.17 ± 13.54 mg GAE/g, significantly higher than the 11.85 ± 9.57 mg GAE/g in CA extract. The ABTS assay confirmed the antioxidant potential with a lower IC<sub>50</sub> value of 1.73 ± 0.41 µg/mL, indicating enhanced radical scavenging activity. Anti-melanogenesis was validated through tyrosinase, showing inhibition rates of 97.97% at the highest concentrations. The anti-inflammatory was evaluated by western blot, which showed decreased expression of iNOS and COX-2. This study demonstrates the green synthesis of CA-AgNPs and its potential biomedical applications. The results of this study demonstrate that biosynthesized CA-AgNPs have key biological applications.

**Keywords** Green synthesis, AgNPs, *Cicer arietinum*, Black roasted gram, Antimicrobial activity, Antioxidant activity, Anti-melanogenic activity, Anti-wrinkle activity, Anti-inflammatory activity

Nanotechnology is a rapidly advancing field in modern material sciences, focusing on the unique properties of nanoparticles that arise from their specific size, distribution, and morphology<sup>1</sup>. Nanomaterials are growing in popularity in biomedical applications, and metal nanoparticles (NPs) such as silver, zinc, gold, and iron are particularly attractive due to their chemical and biological characteristics<sup>2</sup>. Nanocrystalline silver (Ag) particles have found extensive applications in diagnostics, antimicrobials, and therapeutics<sup>3</sup>. Despite their potential, there remains a need for economically viable and environmentally friendly methods to synthesize silver nanoparticles (AgNPs)<sup>4</sup>. Silver, known for its antimicrobial characteristics, has been broadly used in medical processes<sup>1</sup>. In this context, green synthesis of AgNPs using natural resources offers a promising route to develop advanced nanomaterials for various applications while ensuring efficiency and safety<sup>5,6</sup>. Consequently, there has been a growing interest in "green synthesis" methods, which provide a more sustainable alternative approach to NPs production<sup>7</sup>. Green synthesis utilizes biological resources such as plants, microbes, and agricultural byproducts to produce NPs cost-effectively<sup>8</sup>. Medically, AgNPs are being utilized for their therapeutic properties in treating various diseases, including cancer<sup>9-11</sup>. Their unique physical and chemical characteristics enable targeted action

<sup>1</sup>Department of Mechatronics Engineering, Jeju National University, Jeju-si, Republic of Korea. <sup>2</sup>Jeju Inside Agency and Cosmetic Science Center, Department of Chemistry and Cosmetics, Jeju National University, Jeju-si, Republic of Korea. <sup>3</sup>Department of Chemical and Biomolecular Engineering, Yonsei University, Seoul, Republic of Korea. <sup>4</sup>Department of Plant Sciences, Quaid-i-Azam University, Islamabad, Pakistan. <sup>5</sup>Laboratory of Energy Metabolism, Division of Metabolic Disorders, Children's Hospital of Orange County, Los Angeles, CA, USA. <sup>6</sup>These authors contributed equally: Muhammad Awais Farooqi and Sungmin Bae. ✉email: umer.farooqi@choc.org, cghyun@jejunu.ac.kr; cukang@jejunu.ac.kr

and potent anti-cancer effects<sup>12</sup>. The phytochemicals on the surface of the NPs act as antioxidants. AgNPs are renowned for their antimicrobial, antioxidant, anti-melanogenesis, anti-wrinkle, and anti-inflammatory activities<sup>5,8,13</sup>. Traditional methods for synthesizing AgNPs include solution reduction and chemical and photochemical reactions<sup>3</sup>. These methods often involve toxic chemicals that have environmental and health risks. Green synthesis has emerged as an alternative offering better control over the shape and size of NPs<sup>14</sup>. It employs aqueous plant extracts for eco-friendly and compatible with pharmaceutical and biomedical applications, avoiding the toxic chemicals used in traditional chemical synthesis<sup>15</sup>. The advantages of green synthesis over chemical methods include cost-effectiveness, environmental friendliness, and no toxic chemicals<sup>16</sup>. Various plants, including *Mucuna pruriens* and *Mentha arvensis*, have been used to synthesize noble NPs<sup>17</sup>. The use of medicinal plants, fruits, weeds, and spices in NPs production has been extensively explored<sup>18</sup>. Black roasted gram (*Cicer arietinum*) belongs to the Fabaceae family and is nutritionally rich and biomedically significant<sup>19</sup>. They provide high protein, carbohydrates, essential amino acids, polyphenols, and dietary fiber<sup>20</sup>. Roasting, a high-temperature process, improves its functional properties, digestibility, shelf life, and antioxidant properties, making it suitable for ready-to-eat foods. Roasted gram's low glycemic index aids in managing diabetes, while high fiber content promotes weight management, while regular consumption supports cardiovascular health by lowering cholesterol and blood pressure and contributes to bone strength<sup>20–22</sup>. Synthesis of AgNPs using *Cicer arietinum* L. green leaf extract has been previously documented<sup>23</sup>. Our research uses whole black roasted gram (BRG) (*C. arietinum*) as a precursor to producing CA-AgNPs, utilizing a different part of the plant. This approach leverages the unique phytochemical profile present in BRG, which enhances both the synthesis process and the functional properties of the resulting CA-AgNPs. Furthermore, using a commonly available and affordable snack like BRG promotes sustainability by utilizing accessible resources for NP synthesis. The roasting process alters the phytochemical composition of the gram, potentially leading to CA-AgNPs with novel biomedical applications<sup>24</sup>. Plants produce secondary metabolites, such as phenolic compounds, which play a crucial role in NPs synthesis<sup>8</sup>. Phytochemicals present in roasted gram, including polyphenols, flavonoids, and saponins, serve as effective reducing agents, enabling the eco-friendly synthesis of CA-AgNPs through their biochemical interactions and reduction capabilities<sup>18</sup>. This research reports the green synthesis of CA-AgNPs using the black roasted gram (BRG) extract, which acts as a reduction agent for silver ions ( $\text{Ag}^+$ ), and the generation of CA-AgNPs from an aqueous solution of  $\text{AgNO}_3$  and roasted *C. arietinum* extract<sup>19</sup>. The synthesized CA-AgNPs were characterized using UV-Vis spectroscopy, FTIR, XRD, Raman spectroscopy, FESEM, and EDS. The synthesized CA-AgNPs were evaluated for their antimicrobial, antioxidant, anti-melanogenesis, anti-wrinkle, and anti-inflammatory effects. The results demonstrated that CA-AgNPs exhibited significant antimicrobial, antioxidant, anti-melanogenesis, anti-wrinkle, and anti-inflammatory activity, suggesting their potential for advanced biomedical applications. Overall, this study emphasizes the potential of green synthesis of NPs from traditional BRG snacks into valuable CA-AgNPs through a sustainable and cost-effective method for NPs production.

## Materials and methods

### Green synthesized of CA-AgNPs using black roasted grams

The BRG were purchased online from the Coupang market in the Republic of Korea. The whole BRGs were thoroughly rinsed 2–3 times with distilled water to remove any surface dirt and subsequently dried at room temperature to ensure cleanliness and readiness for further processing. When dried and roasted, the grams were crushed using an electric mixer (Philips 3000 series) and stored for later use. 15 g of briefly dried BRG powder was added to 150 mL of distilled water and warmed in a water bath at 55 °C for 15 min. The resulting filtrate (crude extract) was concentrated, freeze-dried, and used for total phenolic contents (TPC), antioxidant, antimicrobial, anti-melanogenesis, and anti-wrinkle assays. Next, prepare to synthesize CA-AgNPs using *C. arietinum* and 10 mM silver nitrate ( $\text{AgNO}_3$ ) solution by dissolving  $\text{AgNO}_3$  in 100 mL of distilled water. Add the BRG extract to the  $\text{AgNO}_3$  solution in a 9:1 ratio under continuous stirring at room temperature for 4 h. After the 4-h continuous stirring reaction, centrifuge the mixture at 5000 rpm for 20 min to collect the CA-AgNPs, discard the supernatant, and wash the NPs three times with distilled water to remove impurities. Finally, dry the CA-AgNPs pellet in a hot air oven at 60–70 °C for 12 h to remove excess moisture and obtain the CA-AgNPs for further characterization analysis and biomedical application as depicted in Fig. 1.

### Physio-chemical characterization techniques

#### UV-visible spectroscopy

The synthesis of CA-AgNPs from *C. arietinum* was conducted by mixing an aqueous extract of BRG with a 10 mM  $\text{AgNO}_3$  solution in a 1:9 ratio, facilitating the reduction process necessary for NPs formation<sup>25</sup>. The reaction mixture was continuously stirred at room temperature for 4 h. The color change indicating formation was observed in the mixture. Samples for UV-Vis spectroscopy were taken at 2 h intervals during the 4 h stirring period<sup>26</sup>. The first sample was taken once the BRG aqueous extract was fully added to the  $\text{AgNO}_3$  solution, followed by samples at 2 h and after 4-h. These samples provided absorbance into the synthesis process. The reduction of  $\text{Ag}^+$  ions to  $\text{Ag}^0$  was observed using PerkinElmer's LAMBDA 850+ UV/Vis spectrophotometer (PerkinElmer, Inc., Waltham, MA, USA).

#### Fourier transform-infrared spectroscopy (FTIR)

Bruker's advanced micro-Fourier transform infrared (FTIR) (Bruker Corporation, Billerica, MA, USA) was used to study the functional groups in the botanical components that cap, reduce, and stabilize CA-AgNPs. FTIR spectroscopy was utilized to detect the functional groups found in the synthesized AgNPs<sup>27</sup>. The functional groups of both the *C. arietinum* extract and the *C. arietinum* (CA) AgNPs were analyzed by examining their absorbance spectrum with a resolution range from 400 to 4000  $\text{cm}^{-1}$ <sup>116</sup>.



**Fig. 1.** The green synthesis of CA-AgNPs from *C. arietinum* (black roasted gram) was conducted utilizing silver nitrate ( $\text{AgNO}_3$ ).

#### X-ray diffraction (XRD)

The X-ray diffractometer (XRD) profiles of the biosynthesized CA-AgNPs were performed using dried CA-AgNPs<sup>28</sup>. Crystallographic data and phase composition analysis were performed using the XRD model Rigaku benchtop (Rigaku Corporation, Tokyo, Japan). XRD analysis was performed to identify the phase composition of CA-AgNPs<sup>25</sup>.

#### Raman analysis

Raman analysis was analyzed in a frequency ranging of  $500\text{--}2000\text{ cm}^{-1}$  using a micro Raman Horiba XploRA (Horiba Scientific, Kyoto, Japan) instrument<sup>14</sup>.

#### FESEM and EDS analysis

The morphological characteristics of the CA-AgNPs were thoroughly examined using scanning electron microscopy (FESEM) with the MIRA3 TESCAN FESEM TESCAN, a.s., Brno, Czech Republic) instrument<sup>29</sup>. Along with FESEM, energy dispersive X-ray spectroscopy (EDS) was used to analyze the chemical composition and measure the relative abundances of elements in the green synthesized CA-AgNPs<sup>7</sup>.

#### Antimicrobial activity

The antimicrobial evaluation was conducted using the following materials and equipment: CA-AgNPs, CA extract, positive controls (Erythromycin, Amphotericin B, and Chloramphenicol), Mueller Hinton agar plates, and cultures of *Propionibacterium acnes* (Gram-positive), *Candida albicans* (Gram-positive), and *Escherichia coli* (Gram-negative). Additional materials included sterile disks, sterile forceps, distilled water, and an incubator set to  $37\text{ }^\circ\text{C}$ <sup>30</sup>. Moreover, LB (BD Biosciences, New Jersey, USA) or BHI (BD Biosciences, New Jersey, USA) agar medium was prepared based on the specific growth requirements of each bacterial strain<sup>31</sup>. Following incubation, the bacterial culture was standardized to ensure a consistent number of strains across all samples for accurate comparison<sup>32</sup>. This standardized culture was then spread evenly on agar plates to ensure a uniform distribution of bacteria across the surface. Subsequently,  $40\text{ }\mu\text{L}$  of  $10\text{ mg/mL}$  solutions of CA-AgNPs, CA extract, and the positive controls were applied to sterilized blank paper disks (DAIHAN Scientific, Gangwon-do, Korea) ( $8\text{ mm}$  diameter,  $1.5\text{ mm}$  thick) using a sterilized pipette tip. The dishes were then incubated upside down at  $37\text{ }^\circ\text{C}$  for  $24\text{ h}$ , after the incubation period, the diameter of the zone of inhibition (ZOI) around each disk was measured

using a transparent ruler. Measurements were recorded in millimeters (mm) and rounded to the nearest 0.5 mm to ensure precision<sup>33</sup>.

### Antioxidant activity

#### *Total phenolic contents assay*

The total phenolic content (TPC) assay was measured using a modification of the Folin–Ciocalteu method, as initially explained by Singleton et al.<sup>34</sup>. For each assay, 900  $\mu\text{L}$  of distilled water (DW), 100  $\mu\text{L}$  of Folin–Ciocalteu reagent (Merck, Darmstadt, Germany), 100  $\mu\text{L}$  of CA-AgNPs and 100  $\mu\text{L}$  of CA extract were mixed and reacted for 3 min at room temperature<sup>35</sup>. After the initial incubation, 200  $\mu\text{L}$  of 2 M sodium carbonate ( $\text{Na}_2\text{CO}_3$ ) (Merck, Darmstadt, Germany) solution was added to the mixture, followed by an additional 700  $\mu\text{L}$  of DW, and incubated in the dark for 1 h at room temperature. Following the incubation period, the absorbance was determined at 700 nm using an Epoch microplate reader (BioTek, Vermont, USA), and this absorbance value was used to quantify the phenolic content. Gallic acid (Merck, Darmstadt, Germany) was used as the standard reference compound for calibration. The TPC of CA-AgNPs and CA extract was then calculated and expressed as milligrams (mg) of gallic acid equivalents (GAE) per gram (g) of sample<sup>36</sup>. The equation used to calculate the total phenolic content was as follows:

$$\text{Total Phenol Content (mg GAE/g)} = \left( \frac{C \times V}{M} \right).$$

(C: Concentration of gallic acid determined from the calibration curve (mg/mL), V: Volume of the extract used in the assay (mL), M: Mass of the extract (g)).

#### *ABTS radical scavenging activity assay*

The ABTS radical scavenging activity assay followed the method performed by Roberta Re et al.<sup>35</sup>. First, a solution containing 7 mM ABTS (Merck, Darmstadt, Germany) was mixed with 2.45 mM potassium persulfate (Merck, Darmstadt, Germany), and the mixture was then allowed to react in the dark for 16 h at room temperature to form  $\text{ABTS}^+$  radicals<sup>37</sup>. Before use, the  $\text{ABTS}^+$  solution was diluted with 95% ethanol (Samcheon, Gyeonggi-do, Korea) to reach an absorbance at 734 nm of  $0.70 \pm 0.02$ , ensuring a consistent starting point for the assay. In a 96-well microplate, 20  $\mu\text{L}$  of CA-AgNPs and CA was added to 180  $\mu\text{L}$  of the  $\text{ABTS}^+$  solution, and mixture was incubated in the dark at room temperature for 10 min. Following the incubation, the absorbance of each well was measured at 734 nm using a microplate reader. L-ascorbic acid (FUJIFILM Wako Chemicals, Tokyo, Japan) was used as a positive control for comparison due to its known antioxidant properties<sup>35</sup>. The radical scavenging activity was calculated using the formula:

$$\text{Radical Scavenging Activity (\%)} = \left( \frac{A_0 - A_s}{A_0} \right) \times 100.$$

( $A_0$ : Absorbance of the control (ABTS solution without sample),  $A_s$ : Absorbance of the sample).

#### *Cupric-reducing antioxidant capacity (CUPRAC) assay*

The CUPRAC assay was conducted based on the method presented by Resat Apak et al.<sup>38</sup>. The working reagent was prepared by mixing equal amounts of 10 mM copper (II) chloride ( $\text{CuCl}_2$ ) (Merck, Darmstadt, Germany), 7.5 mM neocuproine (Merck, Darmstadt, Germany), and 1 M ammonium acetate buffer (pH 7.0) (Merck, Darmstadt, Germany). In a 96-well microplate, 20  $\mu\text{L}$  of CA-AgNPs and CA extract were added to 180  $\mu\text{L}$  of working reagent, and this mixture was then incubated at room temperature for 30 min. Following the incubation, the absorbance of each well was measured at 450 nm using a microplate. L-ascorbic acid was used as a positive control<sup>39</sup>. The antioxidant capacity of the sample was computed using the following formula:

$$\text{Antioxidant Capacity (\%)} = \left( \frac{A_s - A_0}{A_t - A_0} \right) \times 100.$$

( $A_s$ : Absorbance of the sample,  $A_0$ : Absorbance of the blank (solution without sample),  $A_t$ : Absorbance of the positive control (L-ascorbic acid)).

### Tyrosinase inhibition activity assay

The tyrosinase inhibitory activity assay was based on the method adapted from Yeon Mi Kim et al.<sup>40</sup>. L-tyrosine (Merck, Darmstadt, Germany) was used as the substrate for the assay. In a 96-well microplate, 20  $\mu\text{L}$  of CA-AgNPs and CA extract was combined with 70  $\mu\text{L}$  of a 2 mM L-tyrosine solution and 60  $\mu\text{L}$  of 0.1 M potassium phosphate buffer (pH 6.8) (Merck, Darmstadt, Germany). The baseline value was established by the initial absorbance of the mixture which was recorded at 490 nm. Following this, 50  $\mu\text{L}$  of tyrosinase enzyme solution (250 U/mL) (Merck, Darmstadt, Germany) was added to each well, and this mixture was incubated at room temperature for approximately 15 min. The absorbance of the control was monitored and measured using a microplate reader when it reached a value between 0.3 and 0.4 at 490 nm. Arbutin (Merck, Darmstadt, Germany) was used as a positive control in this assay due to its investigated inhibitory effect on tyrosinase<sup>41</sup>. The percentage inhibition of tyrosinase activity was calculated using the following formula:

$$\text{Inhibition (\%)} = \left( \frac{A_c - A_s}{A_c} \right) \times 100.$$

( $A_c$ : Absorbance of the control (without sample),  $A_s$ : Absorbance of the sample).

### Elastase inhibition activity assay

The elastase inhibitory activity assay was carried by the reagents *N*-Succinyl-ala-ala-*p*-nitroanilide (Merck, Darmstadt, Germany) that was previously utilized as the substrate for the assay by Tamsyn S A Thring et al.<sup>42</sup>. In a 96-well microplate, 20  $\mu$ L of CA-AgNPs and CA extract was mixed with 10  $\mu$ L of 6.25 mM *N*-succinyl-ala-ala-*p*-nitroanilide solution and 120  $\mu$ L of 0.1 M Tris-HCl buffer (pH 8.0) (Biosesang, Gyeonggi-do, Korea). The initial absorbance of the mixture was recorded at 405 nm for the blank sample. Following this, 50  $\mu$ L of elastase enzyme solution (0.1 mg/mL) (Merck, Darmstadt, Germany) was added to each well, and this mixture was incubated at room temperature for 15 min. The absorbance of the control was measured using a microplate reader when it reached a value between 0.6 and 0.7 at 405 nm. Ursolic acid (Merck, Darmstadt, Germany) was employed as a positive control due to its potential elastase inhibitory activity<sup>43</sup>. The percentage inhibition of elastase activity was calculated using the formula:

$$\text{Inhibition (\%)} = \left( \frac{A_c - A_s}{A_c} \right) \times 100.$$

( $A_c$ : Absorbance of the control (without sample),  $A_s$ : Absorbance of the sample).

### Anti-inflammatory activity

#### *MTT assay and nitric oxide production test*

Dulbecco's modified Eagle's medium (DMEM; Thermo Fisher Scientific, Massachusetts, USA) medium was supplemented with 10% fetal bovine serum (FBS; Merck, Darmstadt, Germany) and 1% penicillin/streptomycin (Thermo Fisher Scientific, Massachusetts, USA) to make the medium for RAW 264.7 macrophage cell culture<sup>44</sup>. The cells were kept at 37 °C in a humidified atmosphere containing 5% CO<sub>2</sub> (NB-203XL; N-BIOTEK, Bucheon, South Korea). To assess the cytotoxicity of CA-AgNPs and CA extract, the MTT (3-(4,5-dimethylthiazol-2-yl)-2,5-diphenyltetrazolium bromide) (Biosesang, Gyeonggi-do, Korea) assay was utilized<sup>45</sup>. After the initial incubation period, the cells were treated with various concentrations of CA-AgNPs and CA extract and incubated for an additional 24 h. The cell cultures were aspirated, and diluted 0.2 mg/mL MTT solution was added to the medium and incubated for an additional 3 h. After incubation, dimethyl sulfoxide (DMSO; Biosesang, Gyeonggi-do, Korea) was added. To evaluate cell viability, we used DMSO to dissolve purple formazan crystals formed by cells. The absorbance was measured at 570 nm using a microplate reader to calculate the cell viability. Later, the inhibitory activity of nitric oxide (NO) production was accessed. The treated cells with non-cytotoxic concentrations of CA-AgNPs and CA extract were then incubated with 1  $\mu$ g/mL of lipopolysaccharide (LPS) for 24 h. After the incubation period, the samples were mixed with 100  $\mu$ L of the culture supernatant and 100  $\mu$ L of Griess reagent containing 1% sulfanilamide, 0.1% *N*-(1-naphthyl)ethylenediamine, and 2.5% phosphoric acid. This mixture was incubated at room temperature for 10 min and the absorbance was determined at 540 nm<sup>46</sup>. The percentage of NO inhibition was calculated using the following formula:

$$\text{Inhibition (\%)} = \left( \frac{A_c - A_s}{A_c} \right) \times 100.$$

( $A_c$ : Absorbance of the control (LPS-treated cells without sample),  $A_s$ : Absorbance of the sample-treated cells).

#### *Measurement of inflammatory cytokines IL-6 and IL-1 $\beta$ production*

The production of pro-inflammatory cytokines, i.e., IL-6 and IL-1 $\beta$ , which are involved in the inflammatory response, was assessed by enzyme-linked immunosorbent assay (ELISA) kit from BD Biosciences (New Jersey, USA)<sup>47</sup>. The ELISA procedure involved using plates pre-coated with specific antibodies for IL-6 or IL-1 $\beta$ . Serial dilutions of known concentrations of recombinant IL-6 or IL-1 $\beta$  were prepared to generate standard curves. CA-AgNPs and the standards were added to the wells of the ELISA plates and incubated at room temperature for 2 h to allow binding. Following this incubation time, the plates were subjected to multiple washing with wash buffer to remove unbound substances. Later, biotinylated secondary antibodies specific to IL-6 or IL-1 $\beta$  were added to each well, followed by the addition of streptavidin-HRP conjugate<sup>48</sup>. The plates were incubated to allow the formation of the antibody-antigen-enzyme complexes. Subsequently, a substrate solution was added to the wells to develop the colorimetric analysis, which was stopped after 10 min. Absorbance was measured at 450 nm using a microplate reader. The concentrations of IL-6 and IL-1 $\beta$  in CA-AgNPs were calculated based on standard curves obtained from serial dilutions of the recombinant cytokines.

#### *Western blot for anti-inflammatory analysis*

The cells were stimulated with 1  $\mu$ g/mL LPS and incubated for an additional 23 h to induce an inflammatory response<sup>49</sup>. At the end of the treatment period, cells were washed twice with phosphate-buffered saline (PBS; Bioscience, Gyeonggi, Korea) to remove any remaining medium and non-adherent cells. The cells were then lysed using radioimmunoprecipitation assay (RIPA) buffer (50 mM Tris-HCl, pH 7.4, 150 mM NaCl, 1% NP-40, 0.25% sodium deoxycholate, 1 mM EDTA) supplemented with protease and phosphatase inhibitors cocktail (Merck, Darmstadt, Germany). Cells were scraped to collect lysates, which were then transferred to microcentrifuge

tubes. The lysates were incubated on ice for 30 min to ensure complete cell lysis and subsequently centrifuged at 15,000 rpm for 30 min at 4 °C to remove cell debris. Equal amounts of protein (30 µg) from each sample were mixed with 5 × SDS loading buffer and boiled at 100 °C for 3 min to denature the proteins. The samples were first separated on a 10% polyacrylamide gel using SDS-PAGE and then transferred to a PVDF membrane. The membrane was then treated with 5% skim milk in TBS with 0.1% Tween-20 for 1 h at room temperature to block nonspecific binding. After membrane blocking, membranes with primary antibodies against inducible iNOS (1:2000), COX-2 (1:2000), and β-actin (1:2000) were probed and then incubated overnight at 4 °C. Following the primary antibody incubation, the membranes were washed six times with TBST to remove unbound antibodies and then incubated with HRP-conjugated secondary antibodies (1:2000) for 2 h. Following the incubation with the secondary antibody, the membranes underwent an additional six washes with TBST to ensure the removal of any unbound antibodies<sup>50</sup>. Protein bands were visualized using an enhanced chemiluminescence (ECL) system, which emits light upon reaction with a chemiluminescent substrate, allowing for the detection of proteins. Using ImageJ software, the density of the protein bands was quantified to ensure accurate measurement.

### Statistical analysis

The experimental findings were presented as the mean ± standard deviation (SD), derived from a minimum of three independent experiments to ensure the reliability and statistical significance of the data. A detailed statistical analysis was conducted using IBM SPSS software (version 20, SPSS, USA), which provided a robust platform for performing comprehensive data analysis. The significance levels were defined as follows: \* $p < 0.1$ , \*\* $p < 0.01$ , \*\*\* $p < 0.001$ .

## Results and discussion

### UV-Vis spectrum analysis

A notable color change was observed upon adding AgNO<sub>3</sub> to the *C. arietinum* extract, indicating the synthesis of CA-AgNPs<sup>5</sup>. Initially, the reaction mixture exhibited a color change from grey-whitish to brownish-black hue throughout 0, 2, and 4 h, as depicted in Fig. 2. Upon combining the two solutions, a color change from grey-whitish to brownish-black was observed after 4-h, indicating the reduction of Ag<sup>+</sup> ions to Ag<sup>0</sup>. This gradual increase in color intensity signifies that CA-AgNPs were formed as a result of the reduction of Ag<sup>+</sup> ions by bio-organic compounds that are present in the *C. arietinum* extract. Similar observations have been reported in AgNP synthesizing using various plant extracts<sup>8</sup>. AgNPs synthesized from *Moringa oleifera* and *Curcuma longa* also exhibited color changes due to reduced Ag ions, which was attributed to bioactive compounds like tinocordifolioside. Likewise, AgNPs synthesized from the aqueous extract of *Ocimum sanctum*, containing khellin as the main active ingredient, demonstrated successful NPs formation through similar reduction processes. These findings underscore that the bioorganic compounds in *C. arietinum* are responsible for the biosynthesis of CA-AgNPs, as observed through the color changes shown in Fig. 1. UV-visible spectrophotometry was employed to analyze the synthesized CA-AgNPs further. The emergence of a brownish-black hue in the response mixture consisting of AgNO<sub>3</sub> and *C. arietinum* extract was confirmed to be due to the formation of NPs, as shown in Fig. 2A. The UV-Vis spectrum was recorded at 4-h intervals. The color change in the reaction mixture showed how well the Ag<sup>+</sup> ions were reduced by the extract's agents (phenol, flavonoid). The UV-Vis spectrum displayed

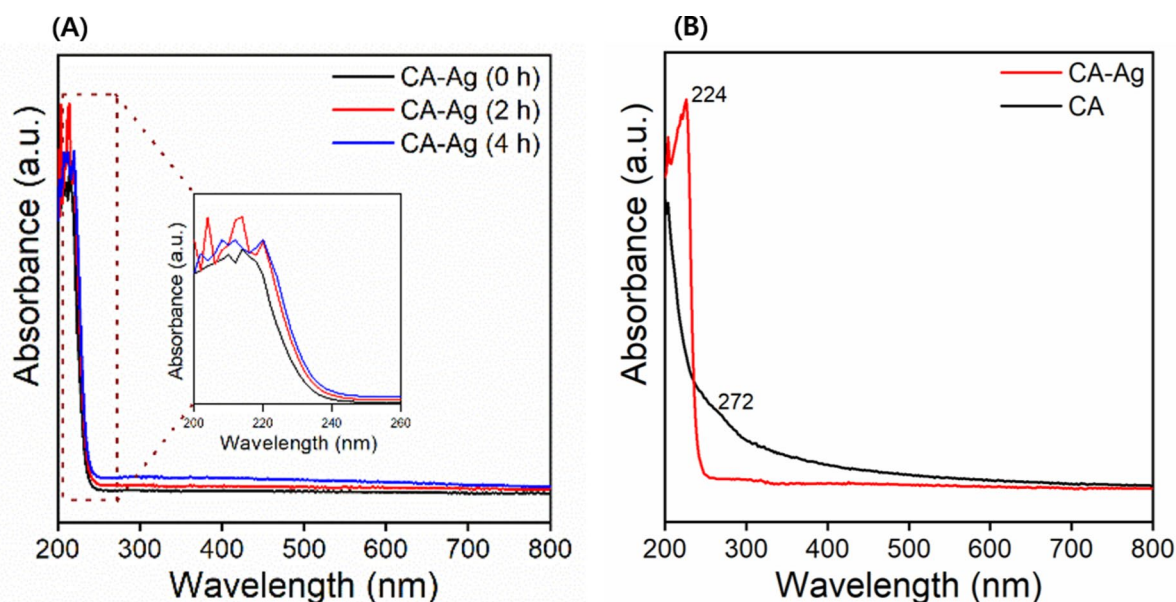


**Fig. 2.** LAMBDA 850 + UV/Vis Spectrophotometer absorbance readings: (A) The time-dependent green synthesis of AgNPs (AgNPs) from *C. arietinum*, and (B) a comparison between CA-AgNPs and *C. arietinum* (CA).

an absorbance peak at 224 nm after 4 h, indicating the presence of CA-AgNPs and the presence of surface plasmon resonance (SPR) associated with these CA-AgNPs (Fig. 2B). The 224 nm peak observed in the UV–Vis spectrum is specific to CA-AgNPs and suggests that the bioorganic compounds in the *C. arietinum* extract helped reduce silver ions ( $\text{Ag}^+$ ) to silver atoms ( $\text{Ag}^0$ )<sup>29</sup>. These silver atoms then acted as starting points for further growth and NPs formation. The 272 nm peak observed in the *C. arietinum* extract is shown in Fig. 2B is attributed to phenolic compounds, which exhibit absorbance in this region due to their aromatic structure. After synthesizing CA-AgNPs, the shift from 272 to 224 nm suggests the formation of new chemical species and modifications in the existing ones due to interactions with silver ions<sup>51</sup>. AgNPs typically exhibit a yellowish-brown color in aqueous solutions due to the SPR. Fig. 2A shows the UV–Vis spectra recorded after 4 h of reaction, where the peak of absorbance at 215 nm suggests the synthesis process of CA-AgNPs<sup>26</sup>.

### FTIR analysis

The FTIR spectra of *C. arietinum*-mediated AgNPs (CA-AgNPs) provide detailed insights into the functional groups involved in synthesizing and stabilizing the NPs<sup>13</sup>. The spectral data was acquired across a range of  $4000\text{ cm}^{-1}$  to  $500\text{ cm}^{-1}$  at a resolution of  $4\text{ cm}^{-1}$ . A peak at  $3286\text{ cm}^{-1}$  was observed, corresponding to the O–H stretching vibration of hydroxyl groups. This peak indicates the presence of polyphenolic compounds or alcohols from the *C. arietinum* extract, which are crucial in reducing Ag ions to AgNPs and stabilizing them. The  $2925\text{ cm}^{-1}$  peak represents the C–H stretching vibration of aliphatic hydrocarbons, suggesting that alkyl groups or fatty acids found in the extract help stabilize the NPs and potentially aid in the reduction process. A peak at  $1561\text{ cm}^{-1}$  corresponds to the C=O stretching vibration of carboxyl groups, which is involved in stabilizing AgNPs and reducing Ag ions. Additionally, the  $1384\text{ cm}^{-1}$  peak is associated with C–O stretching and C–H bending vibrations, indicating the presence of carboxyl or alcohol groups that help in NPs stabilization and Ag ion reduction<sup>26</sup>. The  $1022\text{ cm}^{-1}$  peak signifies C–O stretching vibrations from primary alcohols or phenolic compounds, further supporting their role in the reduction processes. Finally, the peak at  $521\text{ cm}^{-1}$  is due to S–O stretching vibrations, showing the presence of sulfate groups on the CA-AgNPs in the extract, which may influence the functional properties of the NPs<sup>14</sup>. Overall, the FTIR analysis of CA-AgNPs highlights the involvement of functional groups from the *C. arietinum* extract in synthesizing AgNPs. In contrast, the FTIR spectrum of black roasted gram (*C. arietinum*) was studied to investigate the changes in functional groups resulting from the roasting process. A peak at  $640\text{ cm}^{-1}$  was observed, associated with C–H meta-disubstituted benzene aromatic bonds, indicating the formation of aromatic compounds during roasting. A peak at  $1013\text{ cm}^{-1}$  corresponds to the R-NH<sub>2</sub> group of primary amines, reflecting the increase in biogenic amines formed through oxidative decarboxylation of amino acids during the roasting process. The  $1539\text{ cm}^{-1}$  region exhibited absorption bands related to C–C and C–O stretching and C–O–H bending, which signify structural changes in starch due to roasting. Peaks at  $3282\text{ cm}^{-1}$  and  $2923\text{ cm}^{-1}$  represent the stretching vibrations of C–H cis-olefinic groups, indicating alterations in aliphatic groups and amine structures due to the roasting activity. A peak at  $1745\text{ cm}^{-1}$  reveals a decrease in the degree of unsaturation due to the oxidation reaction of the roasted gram<sup>16</sup>. Overall, the FTIR spectrum demonstrates significant changes in the functional groups of roasted grams, including the development of aromatic compounds, increased amine content, and modifications in starch and lipid structures due to the roasting process, as shown in Fig. 3.

### X-ray diffraction (XRD) analysis

The XRD pattern of the CA-AgNPs is depicted in Fig. 4 and spans a  $2\theta$  range from  $20^\circ$  to  $80^\circ$ <sup>8</sup>. It shows distinct peaks at  $33.2^\circ$ ,  $38.4^\circ$ ,  $55.7^\circ$ , and  $66.6^\circ$ , which correspond to the (111), (200), (220), and (311) planes of the face-centered cubic (FCC) structure of Ag. These peaks confirm the crystalline nature of the CA-AgNPs and line up with the standard Joint Committee on Powder Diffraction Standards (JCPDS)<sup>52</sup>. The  $33.2^\circ$  peak indicates the (111) plane and reflects the preferred growth orientation of the NPs, while the  $38.4^\circ$  peak represents the (200) plane. Moreover, the  $55.7^\circ$  and  $66.6^\circ$  peaks correspond to the (220) and (311) planes, respectively, further confirming the presence of the FCC structure. The sharp peaks signify high crystallinity and phase purity of the synthesized CA-AgNPs, with the most intense peak at  $38.4^\circ$  indicating a predominant growth direction along the (111) plane. These findings are consistent with previous studies on AgNPs synthesized using various methods. In contrast, the XRD pattern of the black roasted gram (BRG) is also illustrated in Fig. 4, displays distinct peaks at  $15.4^\circ$ ,  $18.2^\circ$ ,  $20^\circ$ , and  $23.1^\circ$ , which correspond to the (111), (120), (121), and (211) planes, respectively. These peaks reflect the structural characteristics of the BRG, indicating that while some crystalline structure is preserved, the overall crystallinity is less defined compared to the AgNPs<sup>26</sup>. The peak at  $15.4^\circ$  represents the (111) plane, the peak at  $18.2^\circ$  is associated with the (1 2 0) plane, the peak at  $20^\circ$  corresponds to the (121) plane, and the peak at  $23.1^\circ$  relates to the (211) plane, demonstrating that the roasting process retains certain ordered structures. The comparison of the XRD patterns reveals that the CA-AgNPs exhibit a crystalline FCC structure with remarkable phase purity, whereas the BRG shows less intense and broader peaks indicative of retained but less ordered crystalline structures due to the roasting process. This analysis emphasizes the structural modifications between the synthesized CA-AgNPs and the BRG, with the former demonstrating an FCC structure and the latter showing preserved but less defined crystallinity<sup>14</sup>.

### Raman spectra

The Raman spectroscopy analysis of CA-AgNPs is depicted in Fig. 5 and provides the vibrational modes and interactions between *C. arietinum* and CA-AgNPs functional groups present in the BRG extract<sup>8</sup>. The Raman spectra, captured within the range of  $500\text{ cm}^{-1}$  to  $2000\text{ cm}^{-1}$ , exhibit distinct peaks corresponding to various vibrational modes, confirming the synthesis of the CA-AgNPs. The Raman spectra show a peak at  $500\text{ cm}^{-1}$ , which is associated to Ag–S stretching. This peak indicates the formation of Ag–S bonds, showing that

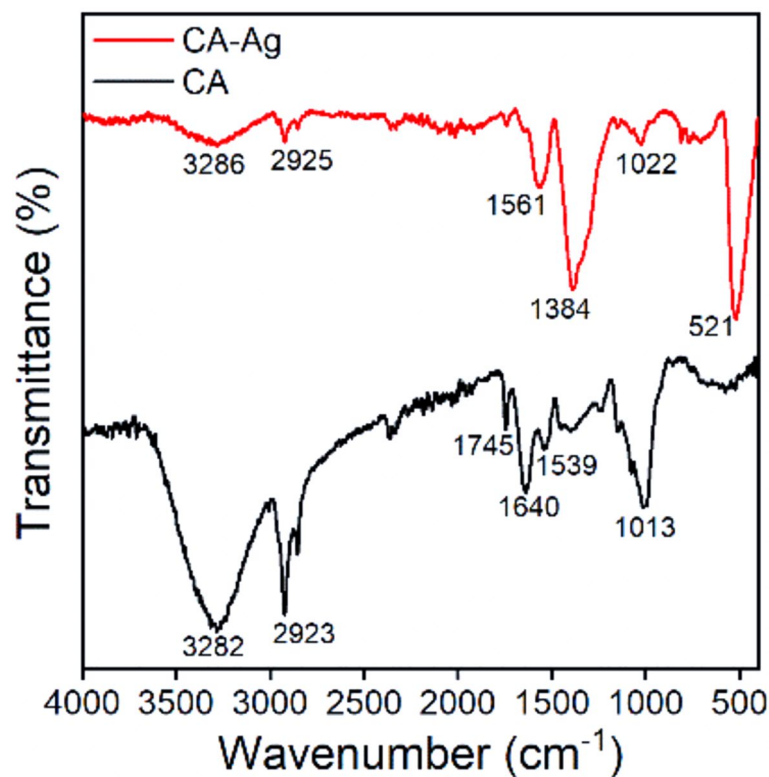


Fig. 3. FTIR Spectra of *Cicer arietinum*(CA) and *C. arietinum*-Mediated AgNPs (CA-AgNPsNPs).

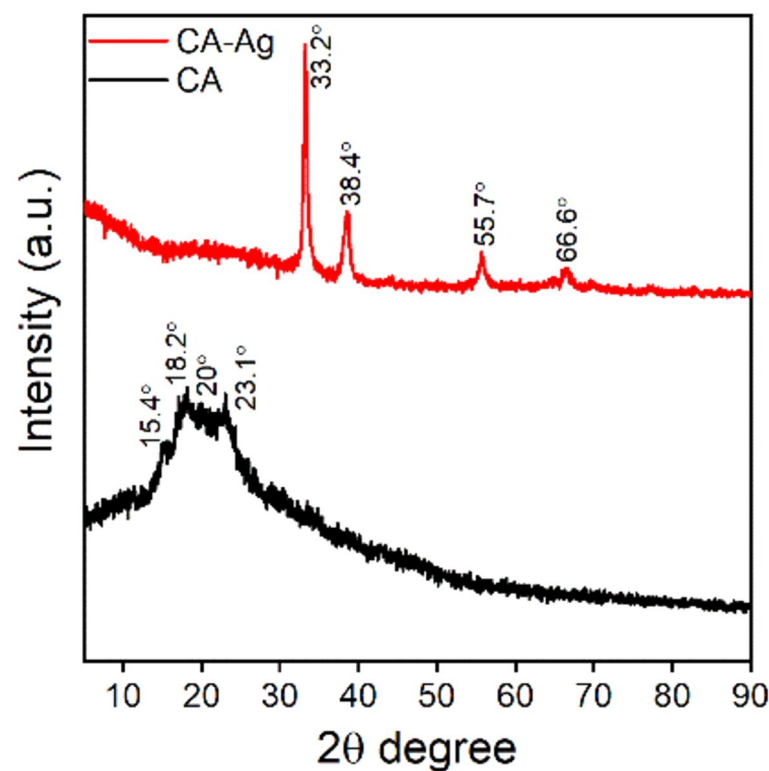
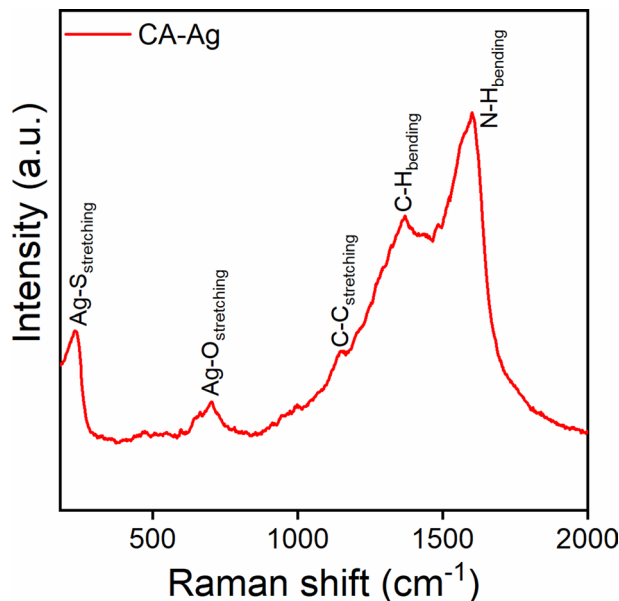


Fig. 4. XRD Patterns of *Cicer arietinum* (CA) and *C. arietinum*-Mediated AgNPs (CA-AgNPsNPs) (A) The XRD pattern of *C. arietinum* (CA) shows peaks corresponding to the (111), (120), (121), and (211) planes. (B) The XRD pattern of CA-AgNPs shows characteristic Bragg peaks for the (111), (200), (220), and (311) planes of the face-centered cubic structure of silver.



**Fig. 5.** Raman Spectra of CA-AgNPs. The spectra show distinctive peaks corresponding to Ag–S stretching, Ag–O stretching, C–C stretching, C–H bending, and N–H bending, indicating the interactions between the CA-AgNPs and the chemical groups found in the *C. arietinum* (CA) extract.

sulfur-containing compounds in the *C. arietinum* extract interact with the CA-AgNPs. These sulfur compounds play a significant role in stabilizing the CA-AgNPs. Peaks at  $662\text{ cm}^{-1}$  and  $961\text{ cm}^{-1}$  are associated with Ag–O stretching, reflecting the interaction between the CA-AgNPs and oxygen-containing chemical groups in the BRG extract<sup>14</sup>. These interactions are crucial for the stabilization and formation of the AgNPs. A peak at  $1165\text{ cm}^{-1}$  corresponds to C–C stretching vibrations, indicating the presence of phenol and flavonoids in the BRG extract. These phenols act as reducing agents during the synthesis of CA-AgNPs, aiding in the reduction of  $\text{Ag}^+$  ions to  $\text{Ag}^0$  and contributing to the stabilization of the CA-AgNPs<sup>14</sup>. The peak at  $1384\text{ cm}^{-1}$  is linked with C–H bending, while a peak at  $1561\text{ cm}^{-1}$  corresponds to N–H bending, showing the presence of amine groups in the BRG extract. Raman spectroscopy results validate the formation of CA-AgNPs and reveal the interactions between the NPs and the functional groups present in the BRG extract. These findings underscore the effectiveness of BRG extract in the green synthesis of CA-AgNPs, demonstrating its sustainable potential and synthesis.

### FESEM analysis and EDS analysis

The morphology and elemental composition of CA-AgNPs were assessed using Field Emission Scanning Electron Microscopy (FESEM) and Energy Dispersive X-ray Spectroscopy (EDS)<sup>19</sup>. FESEM images captured at magnifications of  $1\text{ }\mu\text{m}$ ,  $2\text{ }\mu\text{m}$ ,  $5\text{ }\mu\text{m}$ , and  $500\text{ nm}$  reported that CA-AgNPs exhibited a spherical morphology as shown in Fig. 6. The NPs were dispersed throughout the field, with minimal agglomeration or morphological variations, indicating the synthesis of CA-AgNPs with controlled shape and size. These observations are consistent with similar studies, i.e., using aqueous extracts of *Eriobotrya japonica* leaves, which resulted in particles with a size range from 46 to 70 nm. The average NPs size of around 400–500 nm for CA-AgNPs aligns with previous literature on plant-mediated synthesis of AgNPs<sup>53</sup>. Although some degree of particle aggregation was visible, it was likely due to the evaporation of the solvent during sample preparation. Similar studies, including those focusing on phyto-reducing agents like seed extract, have demonstrated the synthesis of spherical AgNPs with sizes ranging from 100 to 500 nm. The EDS analysis provided information on the elemental composition of the synthesized CA-AgNPs, revealing carbon (C), oxygen (O), and silver (Ag) with weight and atomic percentages of 21.45 wt% and 19.16 at% for C, 5.21 wt% and 8.02 at% for O, and 97.51 wt% and 72.82 at% for Ag, respectively. The highest peak for Ag confirmed the presence of CA-AgNPs<sup>14</sup>. In contrast, the carbon peak indicated that carbon-containing phytoconstituents from the BRG extract were adsorbed on the surface of the NPs. Similar observations of carbon signals in EDS spectra have been reported in other studies using plant extracts for AgNP synthesis, associating these signals to organic compounds from the extracts. The FESEM and EDS analysis provided a comprehensive understanding of the morphology and composition of CA-AgNPs.

### Antimicrobial activity

In this study, the antimicrobial properties of the compounds were tested against three different microorganisms: *P. acnes*, *C. albicans*, and *E. coli*, and positive controls were included to validate the assay<sup>9</sup>. The CA extract was evaluated for their antimicrobial properties but did not show any significant ZOI. This lack of inhibition zones suggests that CA extracts are not effective against the tested bacterial strains, indicating no significant antimicrobial activity. In contrast, the CA-AgNPs demonstrated considerable antimicrobial activity against all three tested microorganisms. Specifically, CA-AgNPs produced ZOI measuring 14 mm for *P. acnes* (Fig. 7A),

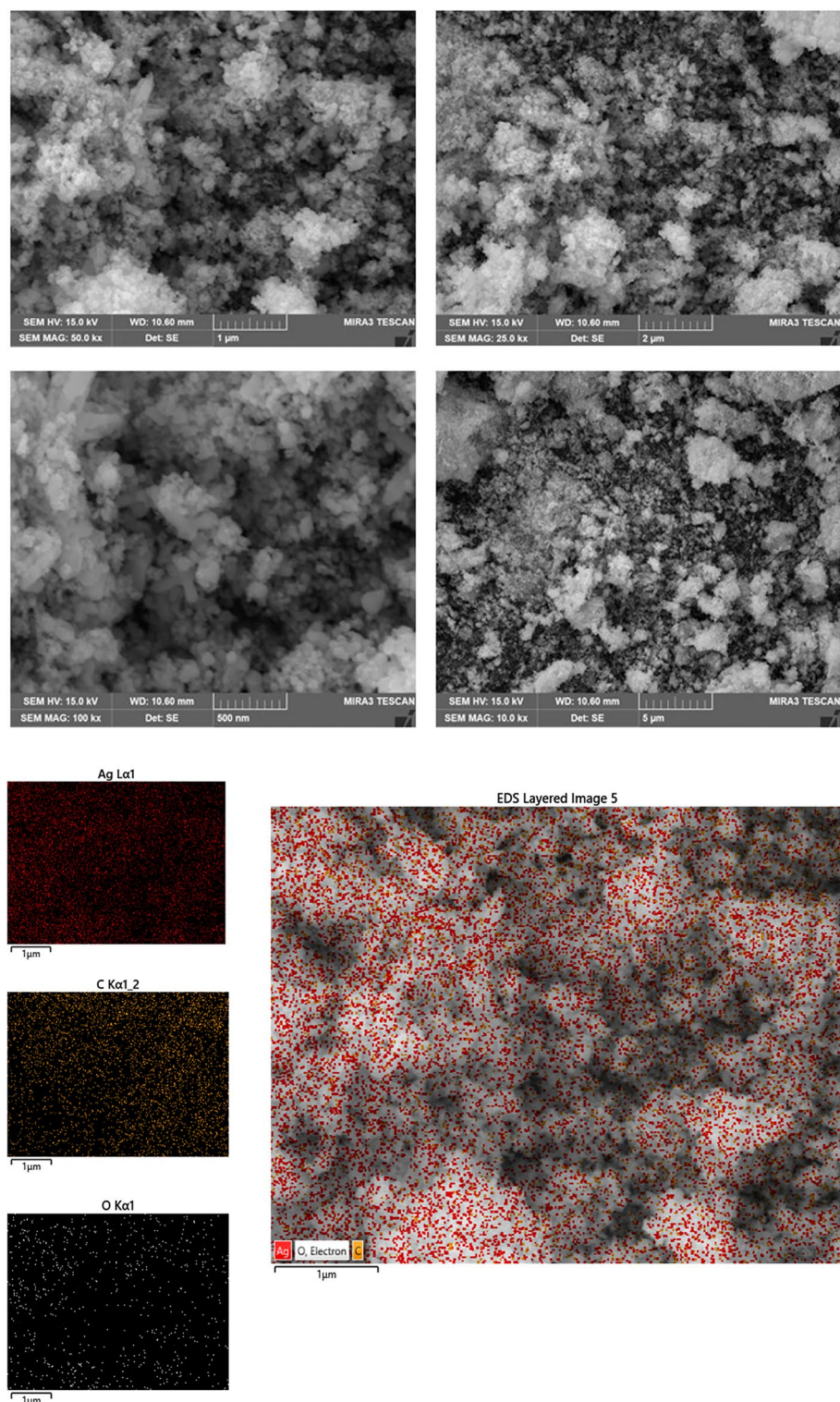


**Fig. 6.** FESEM images of CA-AgNPs: (A) 1  $\mu\text{m}$ , (B) 2  $\mu\text{m}$ , (C) 5  $\mu\text{m}$ , and (D) 500 nm. EDS elemental color mapping of CA-AgNPs showing the distribution of elements: (E) carbon (C), (F) oxygen (O), and (G) silver (Ag). The images confirm the presence of carbon-containing phytoconstituents adsorbed on the surface of the well-dispersed, spherical CA-AgNPs.

18 mm for *C. albicans* (Fig. 7B), and 12 mm for *E. coli* (Fig. 7C). These results indicate that CA-AgNPs have variable antimicrobial efficacy depending on the bacterial strain, showing the highest activity against *C. albicans*

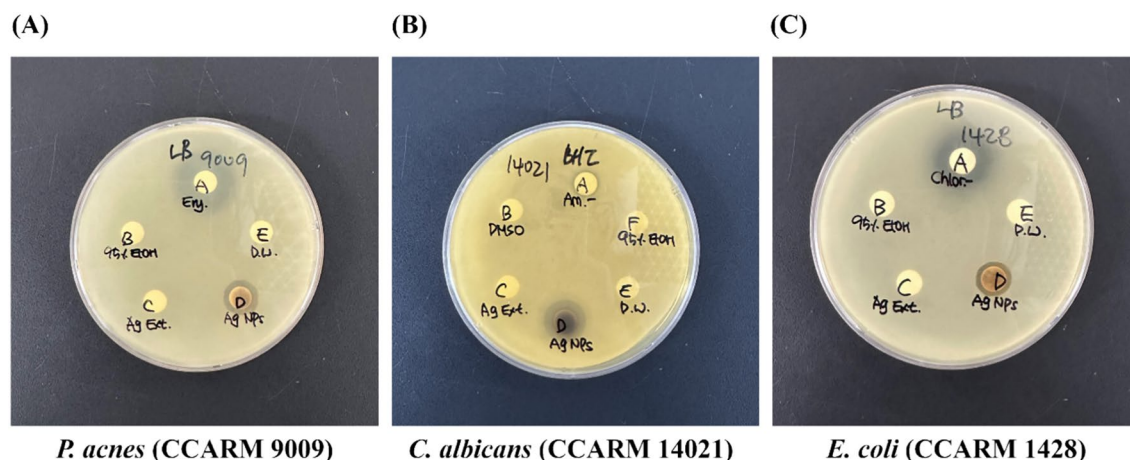


**Fig. 7.** Results of paper disc diffusion on (A) *P. acnes*, (B) *C. albicans*, and (C) *E. coli*. In *P. acnes*, (A) erythromycin, (B) 95% EtOH, (C) CA extract, (D) CA-AgNPs, (E) distilled water. In *C. albicans* (A) amphotericin B, (B) DMSO, (C) CA extract, (D) CA-AgNPs, (E) distilled water, (F) 95% EtOH. In *E. coli*, (A) chloramphenicol, (B) 95% EtOH, (C) CA extract, (D) CA-AgNPs, (E) distilled water.

and the lowest against *E. coli*<sup>54</sup>. The variability in the inhibition zones suggests that the antimicrobial effectiveness of CA-AgNPs is influenced by the type of microorganism, with some strains being more susceptible to CA-AgNPs than others. This study emphasizes the potential of CA-AgNPs as an antimicrobial material with broad-spectrum activity with varying degrees of effectiveness against different bacterial strains<sup>52</sup>.

## Antioxidant activity

### Total phenolic contents

The TPC assay is used to quantify phenolic compounds through a colorimetric reaction. The results are typically expressed in terms of GAE per gram of sample, with gallic acid used as a standard for calibration. In this study, the TPC assay was employed to assess the antioxidant capacity of CA-AgNPs and CA extract<sup>55</sup>. The results demonstrated that CA-AgNPs had the highest TPC, with a value of  $26.17 \pm 13.54$  mg GAE/g, while CA extract exhibited a lower TPC of  $11.85 \pm 9.57$  mg GAE/g (Table 1). These findings indicate a significant difference in the phenolic content between the two samples, with CA-AgNPs showing a higher concentration of phenolic compounds<sup>20</sup>. This difference in phenolic content suggests that CA-AgNPs have a more significant antioxidant potential compared to CA extract. The higher phenolic content in CA-AgNPs is responsible for their enhanced ability to scavenge free radicals and provide antioxidant potential. These results show the importance of phenolic compounds in contributing to the antioxidant properties of the samples and highlight the superior antioxidant potential of CA-AgNPs over CA extract<sup>27</sup>.

### ABTS radical scavenging activity

The ABTS assay was carried out at different concentrations: 6.25, 12.5, 25, 50, and 100  $\mu\text{g}/\text{mL}$ . Both CA-AgNPs and CA extract exhibited an increase in ABTS radical scavenging activity with higher concentrations, indicating their potential as antioxidants<sup>42</sup>. The results revealed that CA-AgNPs demonstrated higher antioxidant activity with a significantly lower  $\text{IC}_{50}$  value of  $1.73 \pm 0.41$   $\mu\text{g}/\text{mL}$  compared to CA extract, which had an  $\text{IC}_{50}$  value of  $24.20 \pm 0.09$   $\mu\text{g}/\text{mL}$  (Fig. 8). The  $\text{IC}_{50}$  value is the concentration required to inhibit 50% of the ABTS radical activity, with a lower  $\text{IC}_{50}$  indicating more potent antioxidant activity<sup>44</sup>. The concentration-dependent increase in ABTS radical scavenging activity observed in both CA-AgNPs and CA extract suggests that both samples contain compounds capable of effectively neutralizing free radicals. The ABTS radical scavenging assay effectively demonstrated the higher antioxidant capacity of CA-AgNPs over CA extract. These findings indicate the potential of CA-AgNPs as a powerful antioxidant, which could be beneficial in various applications, including food preservation, pharmaceuticals, and nutraceuticals<sup>56</sup>.

Sample (mg GAE/g)	Total phenolic content
CA-AgNPs	$26.17 \pm 13.54$
CA	$11.85 \pm 9.57$

**Table 1.** Total phenolic contents of CA-AgNPs and CA extract. Total phenolic contents were measured as described in the method section and reported in milligrams of gallic acid equivalents (GAE) per gram of CA-AgNPs and CA extract. Data represent the average of three independent experiments and are shown as mean  $\pm$  SD.

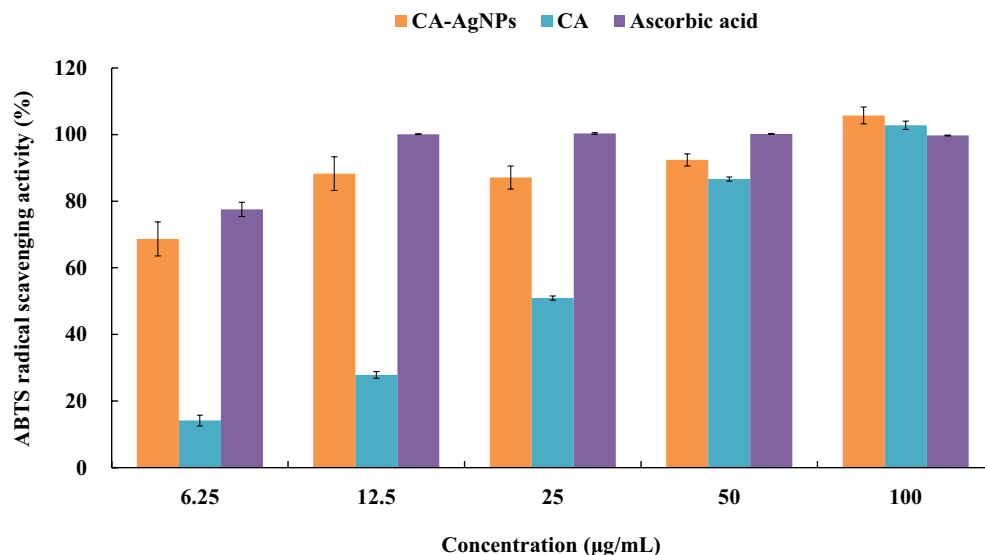


**Fig. 8.** ABTS radical scavenging activity of CA-AgNPs and CA. The ABTS radical scavenging activity was assessed as described in the method section. CA-AgNPs and CA were tested at concentrations ranging from 6.25 to 100 µg/mL, and the percentage inhibition of ABTS<sup>•+</sup> was calculated. Data represent the average of three independent experiments and are shown as mean ± SD. Ascorbic acid was used as a positive control.

#### Cupric-reducing antioxidant capacity assay (CUPRAC)

At all tested sample concentrations, both CA-AgNPs and CA extract showed an increase in absorbance, indicating that higher concentrations of the extracts correspond to more significant antioxidant activity<sup>57</sup>. CA-AgNPs demonstrated a more substantial antioxidant capacity compared to CA extract, as evidenced by a more pronounced increase in absorbance (Fig. 9). This concentration-dependent antioxidant activity suggests that the compounds within CA-AgNPs and CA extract are effective at reducing copper(II) to copper(I), highlighting their potential utility in applications requiring antioxidant properties<sup>58</sup>. The higher CA-AgNPs over CA extract suggests that the presence of silver enhances the antioxidant properties of the compound. The CUPRAC assay effectively demonstrated the antioxidant capabilities of CA-AgNPs and CA extract, with both showing increased activity at higher concentrations<sup>59</sup>.

#### Anti-melanogenesis activity

##### Tyrosinase inhibition activity assay

CA-AgNPs exhibited a concentration-dependent inhibition of tyrosinase enzyme activity, reaching around 97.97% inhibition at the highest concentration of 1000 µg/mL<sup>60</sup>. The IC<sub>50</sub> value of CA-AgNPs was determined to be 69.69 ± 1.89 µg/mL (Fig. 10). This indicates a significantly higher tyrosinase inhibition capacity compared to arbutin, a commonly used skin-whitening agent, which had an IC<sub>50</sub> value of 194.04 ± 2.43 µg/mL and served as a positive control in this assay<sup>40</sup>. The results suggest that CA-AgNPs exhibit significant potential for skin-whitening applications due to their strong inhibitory effect on tyrosinase. Its ability to inhibit tyrosinase activity more effectively than arbutin suggests that CA-AgNPs could be a valuable ingredient in cosmetic formulations aimed at reducing melanin production and achieving a lighter skin tone<sup>61</sup>.

#### Anti-wrinkle activity

##### Elastase inhibition activity assay

The elastase inhibition activity assay is employed to assess the potential anti-wrinkle properties of compounds by evaluating their effectiveness in inhibiting elastase, the enzyme responsible for elastin degradation<sup>43</sup>. Elastin is a crucial protein that maintains skin elasticity, and its breakdown by elastase leads to reduced skin elasticity and the formation of wrinkles. In this assay, sample extracts are incubated with elastase and a synthetic substrate, *N*-Succinyl-ala-ala-ala-*p*-nitroanilide. The enzymatic cleavage of this substrate releases *p*-nitroaniline, which can be measured spectrophotometrically at 405 nm<sup>62</sup>. CA-AgNPs exhibited concentration-dependent inhibition of elastase enzyme activity, reaching around 92.22% inhibition at the highest concentration of 100 µg/mL. The IC<sub>50</sub> value of CA-AgNPs was calculated to be 28.94 ± 1.69 µg/mL (Fig. 11). This indicates a higher elastase inhibition capacity compared to ursolic acid, a known elastase inhibitor, which had an IC<sub>50</sub> value of 43.24 ± 0.19 µg/mL and served as a positive control in this assay<sup>43</sup>.

#### Anti-inflammation activity

##### MTT assay and nitric oxide production test

To analyze the cytotoxicity and anti-inflammatory effects of CA-AgNPs and CA extract, MTT and NO production assays were conducted on RAW 264.7 macrophages<sup>42</sup>. The results of the MTT assay showed that CA-AgNPs

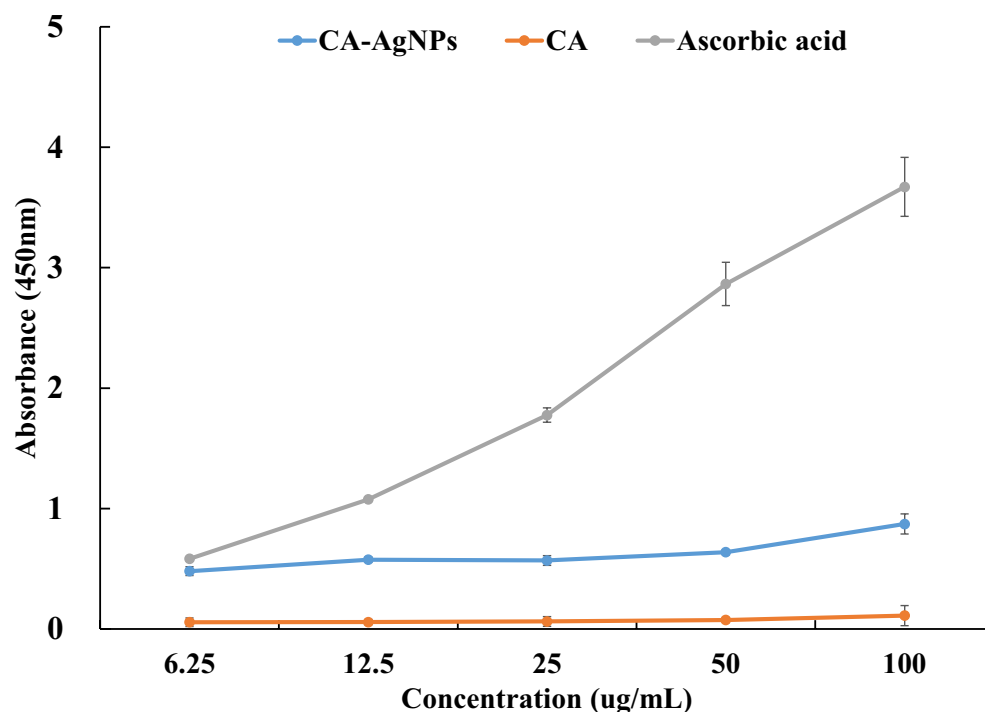


**Fig. 9.** CUPRAC assay of CA-AgNPs and CA. The CUPRAC was measured as outlined in the method section. CA-AgNPs and CA were tested at concentrations ranging from 6.25 to 100  $\mu\text{g}/\text{mL}$ , and the antioxidant capacity was indicated by absorbance measured at 450 nm. Data represent the average of three independent experiments and are presented as mean  $\pm$  SD. Ascorbic acid was used as a positive control.

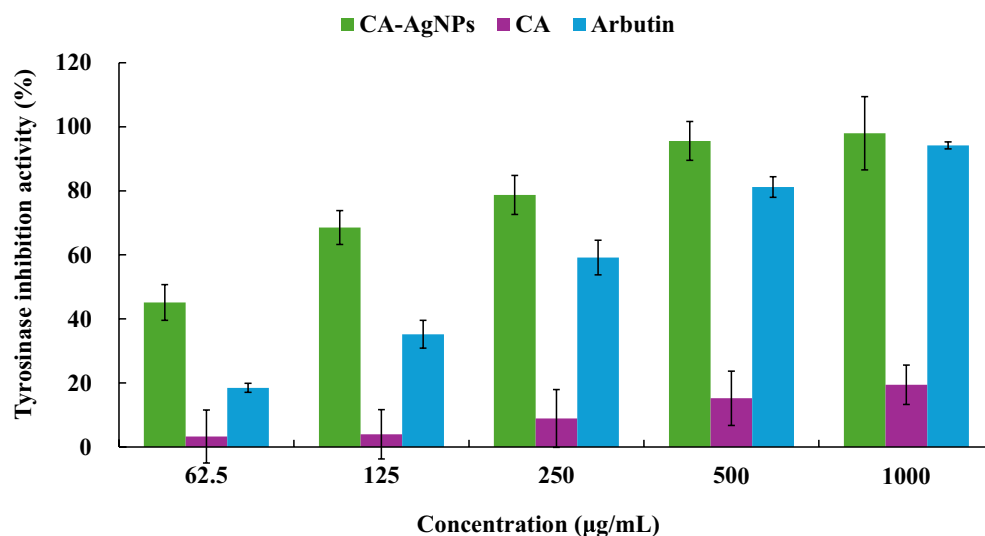


**Fig. 10.** Tyrosinase inhibition activity assay of CA-AgNPs and CA. The tyrosinase inhibition activity was assessed as outlined in the method section. CA-AgNPs and CA were tested at concentrations ranging from 62.5 to 1000  $\mu\text{g}/\text{mL}$ , and the percentage of tyrosinase enzyme inhibition was calculated. Data represent the average of three independent experiments and are presented as mean  $\pm$  SD. Arbutin was used as a positive control.

exhibited cytotoxic effects at a concentration of 20  $\mu\text{g}/\text{mL}$ , with cell viability decreasing to approximately 19.83% (Fig. 12A). While CA extract demonstrated cytotoxic effects at a concentration of 40  $\mu\text{g}/\text{mL}$ , leading to a reduction in cell viability to around 20.48% (Fig. 12B). Based on these findings, NO production measurements were conducted at concentrations below 10  $\mu\text{g}/\text{mL}$  for CA-AgNPs and below 20  $\mu\text{g}/\text{mL}$  for CA extract to avoid cytotoxic effects. The NO production assay showed that NO production was inhibited as the concentration of CA-AgNPs increased<sup>61</sup>. The inhibition rates were approximately 5.54%, 12.56%, 57.74%, and 86.37%

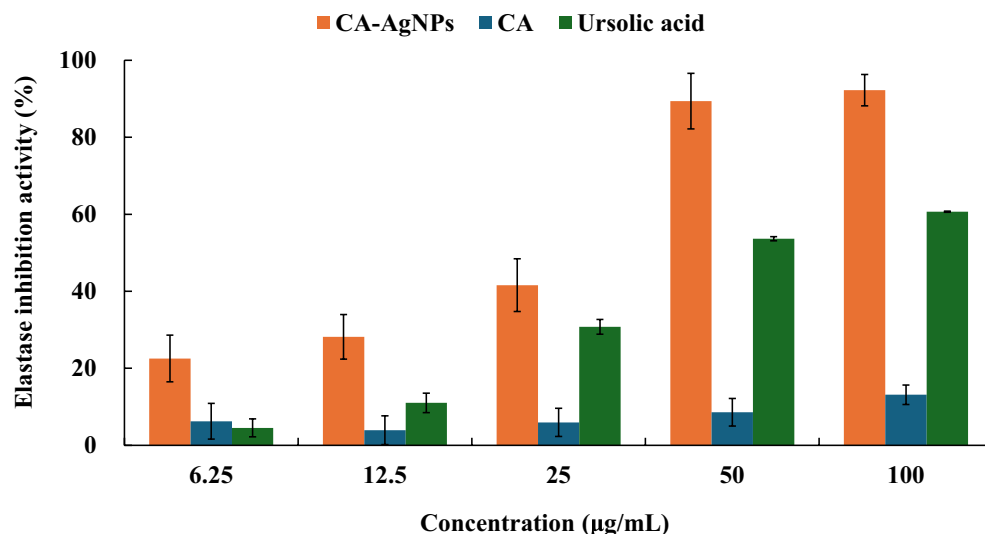


**Fig. 11.** Elastase inhibition activity assay of CA-AgNPs and CA. The elastase inhibition activity was evaluated as detailed in the method section. CA-AgNPs and CA were tested at concentrations ranging from 6.25 to 100 µg/mL, and the percentage of elastase enzyme inhibition was calculated. Data represent the average of three independent experiments and are presented as mean  $\pm$  SD. Ursolic acid was used as a positive control.

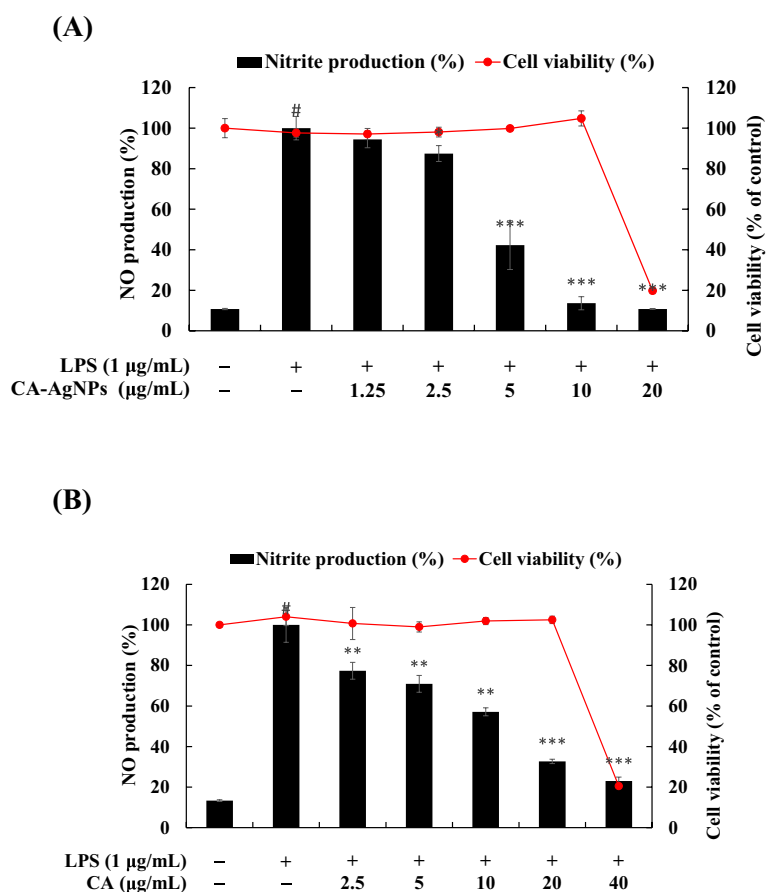


**Fig. 12.** Inhibitory effects of CA-AgNPs and CA on NO production in LPS-stimulated RAW264.7 macrophage cell. RAW264.7 cells were treated with (A) CA-AgNPs and (B) CA, along with LPS (1 µg/mL) for 24 h. Data represent the average of three independent experiments and are presented as mean  $\pm$  SD. <sup>#</sup> $p < 0.001$  compared to the untreated group, \* $p < 0.1$ , \*\* $p < 0.01$ , \*\*\* $p < 0.001$  compared to the LPS alone group.

at concentrations of 1.25, 2.5, 5, and 10  $\mu\text{g/mL}$ , respectively, compared to the group treated with LPS alone (Fig. 12A). Similarly, CA extract exhibited NO inhibition rates of about 22.62%, 29.06%, 42.85%, and 67.28% at concentrations of 2.5, 5, 10, and 20  $\mu\text{g/mL}$ , respectively, compared to the LPS-only group (Fig. 12B). Both CA-AgNPs and CA extract inhibited NO production in a concentration-dependent manner, which confirms their anti-inflammatory activity. These findings suggest that CA-AgNPs and CA can effectively reduce NO production to alleviate the inflammatory response of RAW 264.7 macrophages<sup>63</sup>.

#### Measurement of inflammatory cytokines IL-6 and IL-1 $\beta$ production

The results showed that CA-AgNPs effectively reduced the production of IL-6 with increasing concentrations<sup>44</sup>. Specifically, the reduction was approximately 10.19%, 13.36%, 20.97%, and 23.81% at concentrations of 1.25, 2.5, 5, and 10  $\mu\text{g/mL}$ , respectively, compared to the LPS-only group (Fig. 13A). Similarly, CA-AgNPs decreased the production of IL-1 $\beta$  by approximately 10.20%, 16.86%, 26.22%, and 48.49% at the same respective concentrations (Fig. 13B). These findings suggest that CA-AgNPs have a potent anti-inflammatory effect, as evidenced by their capacity to suppress the production of key inflammatory cytokines IL-6 and IL-1 $\beta$  in a concentration-dependent manner<sup>63</sup>. The reduction in cytokine levels indicates that CA-AgNPs can effectively modulate the inflammatory response, potentially through the inhibition of pathways involved in cytokine synthesis or secretion. The

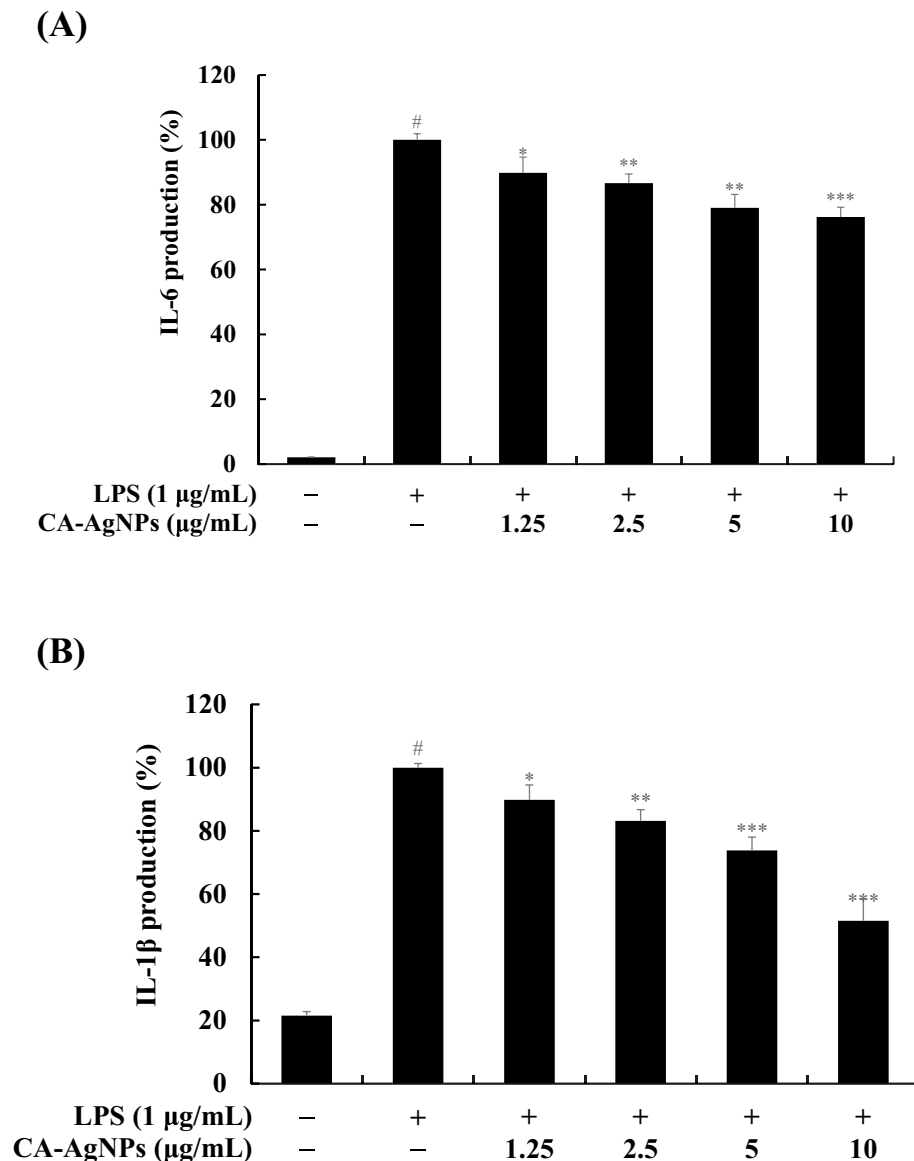


**Fig. 13.** Inhibitory effects of CA-AgNPs on the production of (A) IL-6 and (B) IL-1 $\beta$  in LPS-stimulated RAW264.7 macrophage cells. RAW264.7 cells were treated with CA-AgNPs and LPS (1  $\mu\text{g/mL}$ ) for 24 h. The production of IL-6 and IL-1 $\beta$  was quantified using ELISA. The data show the average of three independent experiments and are shown as mean  $\pm$  SD. <sup>\*</sup> $p < 0.001$  compared to the untreated group, <sup>\*</sup> $p < 0.1$ , <sup>\*\*</sup> $p < 0.01$ , <sup>\*\*\*</sup> $p < 0.01$  compared to the LPS alone group.

production of IL-6 and IL-1 $\beta$  was evaluated by using ELISA in RAW 264.7 macrophages stimulated with LPS, and it was found that CA-AgNPs significantly inhibited the production of these pro-inflammatory cytokines. This suggests that CA-AgNPs possess potent anti-inflammatory properties, making them a potential material for the development of anti-inflammatory therapeutics<sup>50</sup>.

#### Western blot for anti-inflammatory analysis

The effect of CA-AgNPs on the expression levels of iNOS and COX-2 was evaluated using Western blot analysis in LPS-stimulated RAW 264.7 macrophages<sup>49</sup>. The results demonstrated that as the concentration of CA-AgNPs increased, the expression of iNOS and COX-2 proteins decreased (Fig. 14). Specifically, higher concentrations of CA-AgNPs corresponded to greater reductions in the levels of these pro-inflammatory mediators, indicating its potent anti-inflammatory activity<sup>44</sup>. The therapeutic potential of CA-AgNPs in managing inflammatory conditions by modulating crucial inflammatory pathways at the molecular level. The ability of CA-AgNPs to downregulate iNOS and COX-2 expression shows that it could effectively reduce the production of NO. Further studies are required to explore the detailed mechanisms through which CA-AgNPs influence the expression of iNOS and COX-2<sup>63</sup>.

## Discussion

The biosynthesis of CA-AgNPs using BRG extract has been characterized by various analytical techniques, including UV–Vis spectroscopy, FTIR, Raman spectroscopy, FESEM, EDS, and XRD<sup>26</sup>. The comprehensive analysis of these techniques provides an understanding of the properties and formation mechanism of the CA-AgNPs. The UV–Vis spectrum of the CA-AgNPs showed a characteristic SPR peak around 224 nm, confirming the formation of CA-AgNPs. AgNPs typically exhibit a characteristic absorbance peak in the UV–Vis spectrum around 400–450 nm, related to SPR<sup>64</sup>. However, a peak at 224 nm of CA-AgNP indicates functional interactions within the BRG extract, and Ag ions influence the absorption spectrum. The components in the BRG extract, such as phenolics and flavonoids, commonly absorb light around 224 nm<sup>51</sup>. The 224 nm peak is associated with the SPR of the CA-AgNPs, potentially involving ligand-to-metal charge transfer (LMCT) between the CA-AgNPs and the organic molecules from the CA extract<sup>65</sup>. Thus, the shift from 272 nm in the CA extract to 224 nm in the synthesized CA-AgNPs highlights these phytochemicals' significant role in the NP synthesis, resulting in distinct optical properties, which explaining the phenolic-rich plant extracts used in the green synthesis of nanoparticles, where similar shifts in absorbance peaks are observed due to NP formation<sup>66</sup>. FTIR analysis indicated the presence of chemical groups responsible for the stabilization and reduction of CA-AgNPs. Peaks corresponding to O–H stretching (3410 cm<sup>-1</sup>), C–H stretching (2922 cm<sup>-1</sup>), and C=O stretching (1635 cm<sup>-1</sup>) were observed. These functional groups, derived from the phytoconstituents of BRG extract, play a vital role in reducing Ag ions to metallic Ag, and the XRD pattern of the CA-AgNPs exhibited characteristic peaks at 33.2°, 38.4°, 55.7°, and 66.6°, corresponding to the (111), (200), (220), and (311) planes of FCC structure of Ag, respectively<sup>7</sup>. These sharp peaks confirm the high crystallinity and phase purity of the synthesized CA-AgNPs. The intense peak at 38.4° suggests a preferred orientation along the (111) plane, consistent with the formation of highly crystalline CA-AgNPs. Raman spectroscopy further confirmed the successful synthesis and stabilization of CA-AgNPs. The distinctive peaks observed at 226.44 cm<sup>-1</sup> (Ag–S stretching), 487.52 cm<sup>-1</sup>, 662.52 cm<sup>-1</sup>, 961.62 cm<sup>-1</sup> (Ag–O stretching), and 1165.41 cm<sup>-1</sup> (C–C stretching) indicate strong interactions between the CA-AgNPs and the sulfur- and oxygen-containing functional groups from the BRG extract<sup>24</sup>. These interactions are essential for the stabilization and prevention of aggregation of the NPs. The FESEM images of CA-AgNPs demonstrated that the NPs predominantly exhibit a spherical morphology of an average size of about 500 nm<sup>49</sup>. The NPs were dispersed, highlighting the efficiency of BRG extract in controlling the size and shape of the CA-AgNPs. This uniform dispersion and size control are critical for biomedical applications. EDS analysis confirmed the elemental composition of the synthesized CA-AgNPs. The peaks for Ag (97.51% by weight) and the presence of C (21.45%) and O (5.21%) show that organic compounds from the BRG extract are adsorbed on the surface of the CA-AgNPs<sup>67</sup>. The carbon signal indicates the presence of phenol and flavonoids that are responsible for reducing the CA-AgNPs. The combining UV–Vis, FTIR, Raman, FESEM, EDS, and XRD analysis provides comprehensive evidence of the biosynthesis of crystalline CA-AgNPs using *C. arietinum* extract. The phenol found in the extract serves as a reducing agent for CA-AgNPs and maintains uniform size and shape. This green synthesis approach offers a sustainable and efficient method for producing CA-AgNPs with therapeutic applications, including biomedical, environmental, and industrial applications. The results of the analysis presented in this study indicate that CA-AgNPs have significant potential as multifunctional bioactive materials with promising antimicrobial, antioxidant, anti-melanogenesis, anti-wrinkle, and anti-inflammatory properties<sup>59</sup>. The antimicrobial activity of CA-AgNPs was evaluated against three microorganisms, that is, *P. acnes*, *C. albicans*, and *E. coli*, using the paper disk diffusion method. The results showed potent antimicrobial activity of CA-AgNPs, with zones of inhibition (ZOI) of 14 mm against *C. albicans*, 18 mm against *E. coli*, and 12 mm against *P. acnes*. While only the CA extract showed no ZOI, emphasizing the critical role of CA-AgNPs in improving antimicrobial activity. The TPC assay, ABTS radical scavenging assay, and CUPRAC assay were used to evaluate the antioxidant potential of CA-AgNPs. CA-AgNPs exhibited substantially more phenolic content (26.17  $\pm$  13.54 mg GAE/g) compared to CA extract (11.85  $\pm$  9.57 mg GAE/g), showing enhanced antioxidant capacity<sup>23</sup>. AgNPs themselves do not contain phenolic compounds. The observed higher phenolic content in CA-AgNPs indicates the bioactive phenolic compounds present in the BRG (*C. arietinum*) extract that contributed to the synthesis of the CA-AgNPs<sup>68</sup>. During the green synthesis process, these compounds remain associated with the surface of the synthesized CA-AgNPs, leading to increased TPC<sup>69,70</sup>. This increased phenolic content was associated with the more potent radical scavenging activity of CA-AgNPs as evidenced by a lower IC<sub>50</sub> value (1.73  $\pm$  0.41  $\mu$ g/mL) in the ABTS assay compared to CA (24.20  $\pm$  0.09  $\mu$ g/mL). The CUPRAC assay showed a concentration-dependent

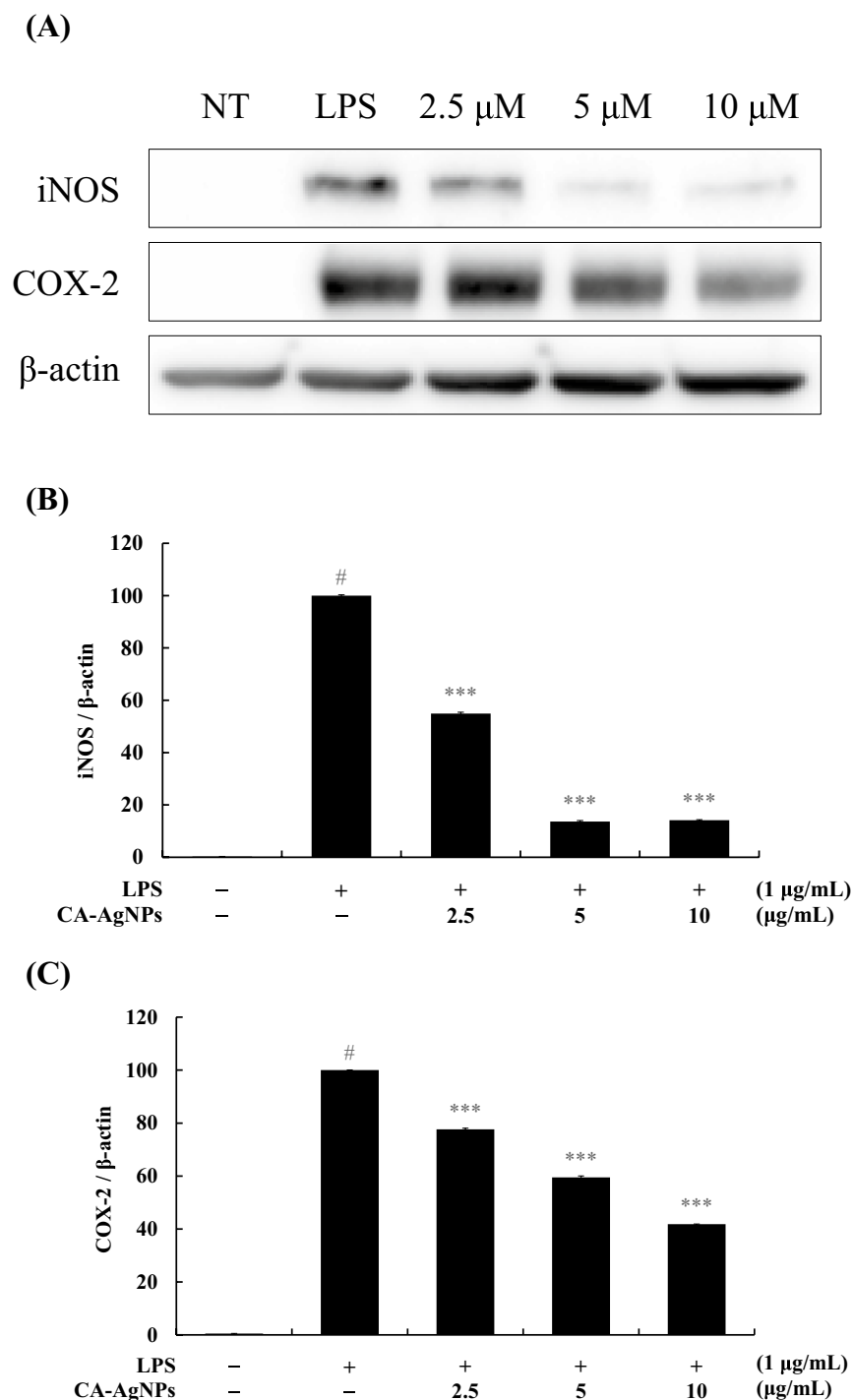


**Fig. 14.** Inhibitory effect of CA-AgNPs on iNOS and COX-2 protein expression in RAW264.7 murine macrophages stimulated with LPS. RAW264.7 cells were treated with CA-AgNPs and LPS (1  $\mu$ g/mL) for 23 h, followed by measurement of iNOS and COX-2 protein expression using western blot analysis. (A) protein bands, (B) iNOS/ $\beta$ -actin ratio, (C) COX-2/ $\beta$ -actin ratio. Data represent the average of three independent experiments and are presented as mean  $\pm$  SD. # $p$  < 0.001 compared to the untreated group, \* $p$  < 0.1, \*\* $p$  < 0.01, \*\*\* $p$  < 0.001 compared to the LPS alone group.

increase in antioxidant ability, additionally confirming the antioxidant activity of CA-AgNPs. The binding of CA-AgNPs seems to significantly enhance the antioxidant properties of CA due to the synergistic effect of enhancing the stability and activity of phenolic compounds. CA-AgNPs exhibited a concentration-dependent tyrosinase inhibition effect, achieving 97.97% inhibition in vitro with an  $IC_{50}$  value of  $69.69 \pm 1.89$   $\mu$ g/mL at

1000 µg/mL. This inhibition is significantly more potent than the standard skin-whitening agent arbutin, which suggests CA-AgNPs could be a practical component in skin-lightening products, providing a natural approach to synthetic drugs with fewer side effects<sup>43</sup>. However, evaluating the safety profile of CA-AgNPs on in vivo applications is crucial to evaluating the side effects of prolonged exposure to high concentrations. Therefore, further research, including preliminary animal studies, is necessary to assess the biocompatibility and safety profile of CA-AgNPs in vivo<sup>71,72</sup>. The tyrosinase inhibitory effect suggests that CA-AgNPs could be a practical component in skin-lightening products, providing a natural approach to synthetic drugs with fewer side effects. CA-AgNPs potently inhibited elastase activity, with an IC<sub>50</sub> value of 28.94 ± 1.69 µg/mL, performing better than ursolic acid, a known elastase inhibitor<sup>73</sup>. The observed concentration-dependent inhibitory effect suggests that CA-AgNPs can effectively maintain skin elasticity by preventing the degradation of elastin, an essential component of the skin structural matrix. The anti-inflammatory properties of CA-AgNPs were investigated using different assays, including MTT, NO production, IL-6 and IL-1β cytokine production, and Western blot analysis<sup>49</sup>. The results demonstrated that CA-AgNPs significantly reduced NO production and inhibited the concentration-dependent levels of the pro-inflammatory cytokines IL-6 and IL-1β in a concentration-dependent manner. Western blot analysis further confirmed the down-regulation of key inflammatory enzymes iNOS and COX-2. These results underscore the potent anti-inflammatory potential of CA-AgNPs, making them suitable for therapeutic applications to manage inflammatory conditions. However, the current findings are primarily based on in vitro assays, which partially replicate in vivo biological interactions. Additional research is required to validate the therapeutic potential of CA-AgNPs in in vivo and organ-on-chip models<sup>74</sup>. Variations in the CA-AgNPs synthesis process, i.e., changes in temperature and duration, may affect the consistency and reproducibility of properties and effectiveness. The antimicrobial and antioxidant activities were evaluated against a limited range of expressions. Expanding these assays could provide a more comprehensive assessment of the therapeutic potential of CA-AgNPs<sup>75,76</sup>.

## Conclusion

In this study, for the first time, whole BRG (*C. arietinum*) was used for the biosynthesis of CA-AgNPs through the reduction of Ag<sup>+</sup> ions and stabilization of CA-AgNPs. The biosynthesized CA-AgNPs showed inhibitory effects against *P. acnes*, *C. albicans*, and *E. coli*. The result showed total phenol content and antioxidant potential, assessed through ABTS and CUPRAC assay. CA-AgNPs also show anti-melanogenesis with Tyrosinase inhibition and anti-wrinkle with elastase inhibition. The MTT assay to evaluate the cell viability and NO production was measured. The cytokines proteins, i.e., IL-6, IL-1β, and then western blot is deployed iNOS, COX-2 has been detected, which shows that CA-AgNPs have significant anti-inflammatory potential. CA-AgNPs biosynthesized using green nanotechnology are excellent candidates for biomedical applications as they have immense potential as a simple, inexpensive, and environmentally friendly approach.

## Data availability

The data will be provided from the corresponding author (cukang@jejunu.ac.kr) on reasonable request.

Received: 22 July 2024; Accepted: 5 September 2024

Published online: 02 October 2024

## References

- Sharma, V. K., Yngard, R. A. & Lin, Y. Silver nanoparticles: Green synthesis and their antimicrobial activities. *Adv. Colloid Interface Sci.* **145**, 83–96 (2009).
- Bhattarai, B., Zaker, Y. & Bigioni, T. P. Green synthesis of gold and silver nanoparticles: Challenges and opportunities. *Curr. Opin. Green Sustain. Chem.* **12**, 91–100 (2018).
- Wei, L. *et al.* Silver nanoparticles: Synthesis, properties, and therapeutic applications. *Drug Discov. Today* **20**, 595–601 (2015).
- Hassan (El-Moushy), R. M. Novel green synthesis of cluster AgNPs by reduction of Silver (I) by vitamin C in presence of alginate surfactant powder in aqueous media: Characteristics and applications. *Environ. Nanotechnol. Monit. Manag.* **22**, 100971 (2024).
- Farooqi, M. A. *et al.* Functionalization of niobium nitrogen-doped titanium dioxide (TiO<sub>2</sub>) nanoparticles with ethanolic extracts of *Mentha arvensis*. *Discov. Nano* **19**, 67 (2024).
- Minhas, L. A. *et al.* Synthesis of silver oxide nanoparticles: A novel approach for antimicrobial properties and biomedical performance, featuring *Nodularia haraviana* from the Cholistan desert. *Microorganisms* **11**, 1–19 (2023).
- Gnanajobitha, G., Annadurai, G. & Kannan, C. Green synthesis of silver nanoparticle using *Elettaria cardamomom* and assessment of its antimicrobial activity. *Int. J. Pharma Sci. Res. (IJPSR)* **3**(3), 323–330 (2012).
- Khuda, F. *et al.* Assessment of antioxidant and cytotoxic potential of silver nanoparticles synthesized from root extract of *Reynoutria japonica* Houtt. *Arab. J. Chem.* **15**, 104327 (2022).
- Kausar, F. *et al.* Evaluation of antimicrobial and anticancer activities of selected medicinal plants of Himalayas, Pakistan. *Plants* **11**, 1–15 (2022).
- Farooqi, M. A. *et al.* Focused Ultrasound as targeted therapy for colorectal cancer: A comprehensive review. *Gastrointest. Disord.* **6**, 380–401 (2024).
- Zorob, T. *et al.* Prevalence and trends in hepatitis B & C virus among blood donors in Pakistan: A regional transfusion center study. *Livers* **3**, 271–281 (2023).
- Farooqi, H. M. U. *et al.* Study of the anticancer potential of plant extracts using liver tumor microphysiological system. *Life* **12**, 1–11 (2022).
- Kaleem, M. *et al.* Biogenic synthesis of iron oxide nanoparticles and experimental modeling studies on the removal of heavy metals from wastewater. *J. Saudi Chem. Soc.* **28**, 101777 (2024).
- Castañeda-Aude, J. E. *et al.* Ultra-small silver nanoparticles: A sustainable green synthesis approach for antibacterial activity. *Antibiotics* **12**, 574 (2023).
- Ahmad, A. *et al.* The effects of bacteria-nanoparticles interface on the antibacterial activity of green synthesized silver nanoparticles. *Microb. Pathog.* **102**, 133–142 (2017).
- Dua, T. K. *et al.* Green synthesis of silver nanoparticles using *Eupatorium adenophorum* leaf extract: Characterizations, antioxidant, antibacterial and photocatalytic activities. *Chem. Pap.* **77**, 2947–2956 (2023).

17. Farooqi, M. A. *et al.* Functionalization of niobium nitrogen-doped titanium dioxide (TiO<sub>2</sub>) nanoparticles by using *Mucuna pruriens* methanolic extracts. *Appl. Nanosci.* **14**, 663–674 (2024).
18. Kausar, F. *et al.* Phytochemical investigation, antimicrobial, antioxidant and anticancer activities of acer cappadocicum gled. *Life* **11**, 1–13 (2021).
19. Kumar, Y., Sharanagat, V. S., Singh, L. & Mani, S. Effect of germination and roasting on the proximate composition, total phenolics, and functional properties of black chickpea (*Cicer arietinum*). *Legum. Sci.* **2**, e20 (2020).
20. Kaur, R. & Prasad, K. Process optimization for the development of traditionally roasted chickpea flour for meal replacement beverages. *Food Chem. Adv.* **3**, 100452 (2023).
21. Farooqi, M. A., Ahsan, A., Yousuf, S., Shakoor, N. & Farooqi, H. M. U. Seroprevalence of hepatitis E virus antibodies (IgG) in the community of Rawalpindi. *Livers* **2**, 108–115 (2022).
22. Imtiaz, C. *et al.* Focused ultrasound, an emerging tool for atherosclerosis treatment: A comprehensive review. *Life* **13**, 1783 (2023).
23. Baran, A. *et al.* Investigation of antimicrobial and cytotoxic properties and specification of silver nanoparticles (AgNPs) derived from *Cicer arietinum* L. green leaf extract. *Front. Bioeng. Biotechnol.* **10**, 855136 (2022).
24. Jogihalli, P., Singh, L., Kumar, K. & Sharanagat, V. S. Physico-functional and antioxidant properties of sand-roasted chickpea (*Cicer arietinum*). *Food Chem.* **237**, 1124–1132 (2017).
25. Mouriya, G. K. *et al.* Green synthesis of *Cicer arietinum* waste derived silver nanoparticle for antimicrobial and cytotoxicity properties. *Biocatal. Agric. Biotechnol.* **47**, 15 (2023).
26. Jain, D. *et al.* Green synthesis of silver nanoparticles using argemone mexicana leaf extract and evaluation of their antimicrobial activities. *Artic. Dig. J. Nanomater. Biostruct.* **5**, 483–489 (2010).
27. Gnanajobitha, G., Annadurai, G. & Kannan, C. Green synthesis of silver nanoparticle using *Elettaria cardamomom* and assesment of its antimicrobial activity. *Int. J. Pharma Sci. Res. (IJPSR)* **3**, 323–330 (2012).
28. Patel, A. M., Dhar, R. & Chakraborty, S. Pulsed light, microwave, and infrared treatments of jaggery: Comparing the microbial decontamination and other quality attributes. *Food Control* **149**, 15 (2023).
29. Singh, R., Singh, R., Parihar, P. & Mani, J. V. Green synthesis of silver nanoparticles using *Solanum sisymbriifolium* leaf extract: Characterization and evaluation of antioxidant, antibacterial and photocatalytic degradation activities. *Process Biochem.* **143**, 337–352 (2024).
30. Balouiri, M., Sadiki, M. & Ibsouda, S. K. Methods for in vitro evaluating antimicrobial activity: A review. *J. Pharm. Anal.* **6**, 71–79. <https://doi.org/10.1016/j.jppha.2015.11.005> (2016).
31. Clsi. *M02-A11: Performance Standards for Antimicrobial Disk Susceptibility Tests; Approved Standard—Eleventh Edition.*
32. Kaningini, A. G., Motlhalamme, T., More, G. K., Mohale, K. C. & Maaza, M. Antimicrobial, antioxidant, and cytotoxic properties of biosynthesized copper oxide nanoparticles (CuO-NPs) using *Athrixia phylicoides* DC. *Heliyon* **9**, e15265 (2023).
33. Bae, S.-E., Bae, S., Park, S. J., Lee, P. & Hyun, C.-G. Microbial consortium of jeju traditional fermented foods and their cosmetic ingredient potential. *Fermentation* **10**, 345 (2024).
34. Pérez, M., Dominguez-López, I. & Lamuela-Raventós, R. M. The chemistry behind the Folin–Ciocalteu method for the estimation of (poly)phenol content in food: Total phenolic intake in a mediterranean dietary pattern. *J. Agric. Food Chem.* **71**, 17543–17553 (2023).
35. Re, R. *et al.* Antioxidant activity applying an improved ABTS radical cation decolorization assay. *Free Radic. Biol. Med.* **26**, 1231–1237 (1999).
36. Malta, L. G. & Liu, R. H. Analyses of total phenolics, total flavonoids, and total antioxidant activities in foods and dietary supplements. *Encycl. Agric. Food Syst.* <https://doi.org/10.1016/B978-0-444-52512-3.00058-9> (2014).
37. Miller, N. J. & Rice-Evans, C. A. Factors influencing the antioxidant activity determined by the ABTS.+ radical cation assay. *Free Radic. Res.* **26**, 195–199 (1997).
38. Apak, R., Güçlü, K., Özyürek, M. & Karademir, S. E. Novel total antioxidant capacity index for dietary polyphenols and vitamins C and E, using their cupric ion reducing capability in the presence of neocuproine: CUPRAC method. *J. Agric. Food Chem.* **52**, 7970–7981 (2004).
39. Güçlü, K., Altun, M., Özyürek, M., Karademir, S. E. & Apak, R. Antioxidant capacity of fresh, sun- and sulphited-dried Malatya apricot (*Prunus armeniaca*) assayed by CUPRAC, ABTS/TEAC and folin methods. *Int. J. Food Sci. Technol.* **41**, 76–85 (2006).
40. Kim, Y. J. & Uyama, H. Tyrosinase inhibitors from natural and synthetic sources: Structure, inhibition mechanism and perspective for the future. *Cell. Mol. Life Sci.* **62**, 1707–1723. <https://doi.org/10.1007/s00018-005-5054-y> (2005).
41. Murata, K. *et al.* Tyrosinase inhibitory activity of extracts from *Prunus persica*. *Separations* **9**, 107 (2022).
42. Thring, T. S. A., Hili, P. & Naughton, D. P. Anti-collagenase, anti-elastase and anti-oxidant activities of extracts from 21 plants. *BMC Complement. Altern. Med.* **9**, 27 (2009).
43. Chiocchio, I. *et al.* Screening of a hundred plant extracts as tyrosinase and elastase inhibitors, two enzymatic targets of cosmetic interest. *Ind. Crops Prod.* **122**, 498–505 (2018).
44. Suriyaprom, S. *et al.* Antioxidant and anti-inflammatory activity on LPS-stimulated RAW 264.7 macrophage cells of white mulberry (*Morus alba* L.) leaf extracts. *Molecules* **28**, 4395 (2023).
45. Gamal El-Din, M. M. *et al.* Inhibitory effects of triarylpyrazole derivatives on LPS-induced nitric oxide and PGE2 productions in murine RAW 264.7 macrophages. *Bioorgan. Med. Chem. Lett.* **30**, 126884 (2020).
46. He, J. W. *et al.* Anti-inflammatory and antioxidant activities of flavonoids from the flowers of: *Hosta plantaginea*. *RSC Adv.* **8**, 18175–18179 (2018).
47. Yang, L. *et al.* Hostaflavanol A, a new anti-inflammatory and antioxidant activities flavanol from the flowers of *Hosta plantaginea*. *Med. Chem. Res.* **29**, 426–430 (2020).
48. He, W. & Frost, M. C. Direct measurement of actual levels of nitric oxide (NO) in cell culture conditions using soluble NO donors. *Redox Biol.* **9**, 1–14 (2016).
49. Pudla, M., Srisaowakarn, C. & Utaisincharoen, P. NLRP12 negatively modulates inducible nitric oxide synthase (iNOS) expression and tumor necrosis factor- $\alpha$  production in *Porphyromonas gingivalis* LPS-treated mouse macrophage cell line (RAW264.7). *Inflamm. Res.* **68**, 841–844 (2019).
50. Fang, Y., Yang, L. & He, J. Plantaneone C attenuates LPS-stimulated inflammation by inhibiting NF- $\kappa$ B/iNOS/COX-2/MAPKs/Akt pathways in RAW 264.7 macrophages. *Biomed. Pharmacother.* **143**, 112104 (2021).
51. Ihsan, M. *et al.* Biologically synthesized silver nanoparticle-based colorimetric sensor for the selective detection of Zn<sup>2+</sup>. *RSC Adv.* **5**, 911158–911165 (2015).
52. Raza, H. *et al.* Effects of ball-milling on physicochemical, thermal and functional properties of extruded chickpea (*Cicer arietinum* L.) powder. *CYTA J. Food* **17**, 563–573 (2019).
53. Sofi, S. A. *et al.* Impact of germination on structural, physicochemical, techno-functional, and digestion properties of desi chickpea (*Cicer arietinum* L.) flour. *Food Chem.* **405**, 135011 (2023).
54. Nasir, A. *et al.* Advances in nanotechnology-assisted photodynamic therapy for neurological disorders: A comprehensive review. *Artif. Cells Nanomed. Biotechnol.* **52**, 84–103. <https://doi.org/10.1080/21691401.2024.2304814> (2024).
55. Mouriya, G. K. *et al.* Green synthesis of *Cicer arietinum* waste derived silver nanoparticle for antimicrobial and cytotoxicity properties. *Biocatal. Agric. Biotechnol.* **47**, 102573 (2023).
56. Kut, K., Cieniek, B., Stefaniuk, I., Bartosz, G. & Sadowska-Bartos, I. A modification of the ABTS• decolorization method and an insight into its mechanism. *Processes* **10**, 1288 (2022).

57. Hyun, S. B., Bae, S. & Hyun, C. G. Antioxidant activities of jeju wax apple (*Syzygium samarangense*) and safety of human keratinocytes and primary skin irritation test. *Cosmetics* **7**, 39 (2020).
58. Apak, R., Güçlü, K., Özyürek, M., Esin Karademir, S. & Erçğ, E. The cupric ion reducing antioxidant capacity and polyphenolic content of some herbal teas. *Int. J. Food Sci. Nutr.* **57**, 292–304 (2006).
59. Bener, M., Özyürek, M., Güçlü, K. & Apak, R. Novel optical fiber reflectometric CUPRAC sensor for total antioxidant capacity measurement of food extracts and biological samples. *J. Agric. Food Chem.* **61**, 8381–8388 (2013).
60. Koley, R., Mondal, A. & Mondal, N. K. Green synthesized silver nanoparticles mediated regulation on hydrolytic enzymes and ROS homeostasis promote growth of three pulses (*Cicer arietinum* L., *Pisum sativum* L., and *Vigna radiata* L.). *Energy Ecol. Environ.* **8**, 537–555 (2023).
61. Bae, S., Lee, J. N. & Hyun, C. G. Anti-melanogenic and anti-inflammatory effects of 2'-hydroxy-4',6'-dimethoxychalcone in B16F10 and RAW264.7 Cells. *Curr. Issues Mol. Biol.* **46**, 6018–6040 (2024).
62. Fayad, S., Tannoury, M., Morin, P. & Nehmé, R. Simultaneous elastase-, hyaluronidase- and collagenase-capillary electrophoresis based assay. Application to evaluate the bioactivity of the red alga *Jania rubens*. *Anal. Chim. Acta* **1020**, 134–141 (2018).
63. Bae, S. & Hyun, C. G. The effects of 2'-hydroxy-3,6'-dimethoxychalcone on melanogenesis and inflammation. *Int. J. Mol. Sci.* **24**, 10393 (2023).
64. Ratan, Z. A. *et al.* Green chemistry synthesis of silver nanoparticles and their potential anticancer effects. *Cancers (Basel)* **12**, 855 (2020).
65. Rakesh, B. *et al.* Antibacterial activity and spectroscopic characteristics of silver nanoparticles synthesized via plant and invitro leaf-derived callus extracts of *Mucuna pruriens* (L.) DC. *S. Afr. J. Bot.* **148**, 251–258 (2022).
66. Dhaka, A., Chand Mali, S., Sharma, S. & Trivedi, R. A review on biological synthesis of silver nanoparticles and their potential applications. *Results Chem.* **6**, 101108 (2023).
67. Jogihalli, P., Singh, L., Kumar, K. & Sharanagat, V. S. Novel continuous roasting of chickpea (*Cicer arietinum*): Study on physico-functional, antioxidant and roasting characteristics. *Lwt* **86**, 456–464 (2017).
68. Vanlalveni, C. *et al.* Green synthesis of silver nanoparticles using plant extracts and their antimicrobial activities: A review of recent literature. *RSC Adv.* **11**, 2804–2837 (2021).
69. Tripathi, D. & Pandey-Rai, S. Chapter 22—impacts of green synthesized silver nanoparticles with natural bioactive compounds on plant's developmental behavior. In (eds Sinha, R. P. & Häder, D. -P.B.T.-N.B.C.) 435–452 (Academic Press, London, 2021).
70. Salayová, A. *et al.* Green synthesis of silver nanoparticles with antibacterial activity using various medicinal plant extracts: Morphology and antibacterial efficacy. *Nanomaterials* **11**, 1005 (2021).
71. Niloy, M. S. *et al.* Synthesis of biogenic silver nanoparticles using *Caesalpinia digyna* and investigation of their antimicrobial activity and in vivo biocompatibility. *ACS Appl. Bio Mater.* **3**, 7722–7733 (2020).
72. Farooqi, H. M. U. *et al.* Acute neuro-biochemical changes induced by nitrogen-tungsten co-doped titanium dioxide nanoparticles. *Appl. Biol. Chem.* **66**, 83 (2023).
73. Landa-Cansigno, C. *et al.* The antioxidant and anti-elastase activity of the brown seaweed *Sargassum horridum* (Fucales, Phaeophyceae) and their early phenolics and saponins profiling for green cosmetic applications. *Algal Res.* **75**, 103271 (2023).
74. Farooqi, M. A., Kang, C. U. & Choi, K. H. Organ-on-chip: Advancing nutraceutical testing for improved health outcomes. *ACS Omega* **8**, 31632–31647 (2023).
75. Mohammed, A. A. *et al.* Investigating the antimicrobial, antioxidant, and anticancer effects of *Elettaria cardamomum* seed extract conjugated to green synthesized silver nanoparticles by laser ablation. *Plasmonics* **19**, 1187–1200 (2024).
76. Kebede, O. G., Pasaogullari Aydinlik, N., Oba, O. A. & Ertekin, E. Green synthesis and characterization of limonium sinuatum silver nanoparticles (AgNPs) for antioxidant and antimicrobial applications. *Anal. Lett.* **57**, 2773–2785 (2024).

## Acknowledgment

Not applicable.

## Author contributions

Conceptualization and methodology, M.A.F.; validation, H.M.U.F. and S.B., S.K. and S.B.; formal analysis, H.M.U.F. and F.K., resources, C.U.K. writing—original draft preparation, M.A.F. and S.B., writing—review and editing, F.K.; visualization, S.K. AND S.B., supervision; H.M.U.F., C.G.H., and administration, C.U.K.

## Competing interests

The authors declare no competing interests.

## Additional information

**Correspondence** and requests for materials should be addressed to H.M.U.F., C.G.H. or C.U.K.

**Reprints and permissions information** is available at [www.nature.com/reprints](http://www.nature.com/reprints).

**Publisher's note** Springer Nature remains neutral with regard to jurisdictional claims in published maps and institutional affiliations.

**Open Access** This article is licensed under a Creative Commons Attribution-NonCommercial-NoDerivatives 4.0 International License, which permits any non-commercial use, sharing, distribution and reproduction in any medium or format, as long as you give appropriate credit to the original author(s) and the source, provide a link to the Creative Commons licence, and indicate if you modified the licensed material. You do not have permission under this licence to share adapted material derived from this article or parts of it. The images or other third party material in this article are included in the article's Creative Commons licence, unless indicated otherwise in a credit line to the material. If material is not included in the article's Creative Commons licence and your intended use is not permitted by statutory regulation or exceeds the permitted use, you will need to obtain permission directly from the copyright holder. To view a copy of this licence, visit <http://creativecommons.org/licenses/by-nc-nd/4.0/>.

© The Author(s) 2024